MULTISCALE MODEL. SIMUL.
Vol. 10, No. 1, pp. 82–110

BUCKLING INSTABILITY OF VIRAL CAPSIDS—A CONTINUUM APPROACH*

SEBASTIAN ALAND†, ANDREAS RÄTZ‡, MATTHIAS RÖGER‡, AND AXEL VOIGT§

Abstract. The crystallographic structure of spherical viruses is modeled using a multiscale approach combining a macroscopic Helfrich model for morphology evolution with a microscopic approximation of a classical density functional theory for the protein interactions. The derivation of the model is based on energy dissipation and conservation of protein number density. The resulting set of equations is solved within a diffuse domain approach using finite elements and shows buckling transitions of spherical shapes into faceted viral shapes.

Key words. viral capsids, ordering on curved surfaces, phase field crystal, Helfrich model

AMS subject classifications. 35R01, 35K25

DOI. 10.1137/110834718

1. Introduction.

A capsid is the protein shell of a virus. It encloses the genetic material of a virus and protects it from enzymatic digestion. The capsid proteins are expressed from the DNA or RNA genome of the virus, and in physiological conditions self-assemble into very efficient structures which can withstand high forces while at the same time effectively disassemble to allow the viral genome to be released in the host cell. Capsids are broadly classified according to their structure. Most viral capsids are spherical. The crystallographic structures of spherical viruses have been extensively investigated by techniques such as X-ray spectroscopy and cryotransmission electron microscopy. Structural analyses of major capsid protein architectures have been used to categorize viruses into families, and the analyzed structure of the capsid forms part of the core knowledge of modern virology.

The capsid proteins are grouped in subunits called capsomers, which are oligomers made of either five (pentamer) or six (hexamer) proteins. Spherical viruses typically possess icosahedral symmetry with 12 pentamers located at the vertices of a regular icosahedron and hexamers at the faces. The diameters of spherical viruses span the range from 10 to 100 nm. While small capsids are almost perfectly spherical, large viruses, such as the bacteriophage HK97 or the phycodnavirus, typical exhibit a faceted geometry with nearly flat portions separated by ridges and sharp corners corresponding to the 12 pentamers. One explanation for the transition between spherical and faceted shapes is a buckling transition resulting from a balance between the stretching energy associated with the pentamers in capsomer lattices and the bending elasticity of the viral capsid [21]. Viruses with different overall capsid size are composed of nearly identical monomers, and the capsid proteins have nearly identical

*Received by the editors May 19, 2011; accepted for publication (in revised form) October 19, 2011; published electronically March 6, 2012. The first and fourth authors acknowledge support from the German Science Foundation through grants Vo899/6-2 and Vo899/11-1.
http://www.siam.org/journals/mms/10-1/83471.html

†Institut für Wissenschaftliches Rechnen, Technische Universität Dresden, 01062 Dresden, Germany (sebastian.aland@tu-dresden.de).

‡Mathematische Fakultät, Technische Universität Dortmund, Vogelpothsweg 87, 44227 Dortmund, Germany (andreas.raetz@tu-dortmund.de, matthias.roeger@tu-dortmund.de).

§Institut für Wissenschaftliches Rechnen, Technische Universität Dresden, 01062 Dresden, Germany, and Center of Advanced Modeling and Simulation, 01062 Dresden, Germany (axel.voigt@tu-dresden.de).

size, weight, composition, and folded structure [26]. This allows us to view the 12 isolated points of fivefold symmetry as disclinations in an otherwise sixfold medium. As in flat space in which the large strain associated with an isolated disclination leads to buckling into a conical shape, the icosahedral shell becomes aspherical if the Föppl–von Karman number $\gamma = YR^2/\kappa_N \gg 1$, with Y the Young's modulus, κ_N the normal bending rigidity, and R the radius. Most viruses have $\gamma \leq 150$ with a close-to-spherical shape, or $200 \leq \gamma \leq 1500$ with a strong buckling effect. In [21] the mean square asphericity is computed as a function of γ, using the classical Caspar and Klug model [8] in combination with a discrete Helfrich model [18]. The icosahedral shape of the capsid is thereby given.

We will follow a different approach to model the buckling transition, which is not restricted to spherical or almost spherical shapes and does not impose icosahedral structure. We therefore postulate that the condensed matter order of the capsid proteins induces an anisotropy in the bending rigidity which can lead to morphological changes. We consider the classical Helfrich model [18], which is based on the assumption that the surface energy associated with bending of the capsid can be expanded in the mean curvature $H = \kappa_1 + \kappa_2$ and the Gaussian curvature $K = \kappa_1\kappa_2$, with $\kappa_{1,2}$ the principle curvatures of a surface Γ. The energy $\mathcal{F}_{Helfrich}$ consists of the following parts:

- the normal bending energy,

$$\mathcal{F}_{Helfrich,B}(\Gamma) = \frac{1}{2}\int_\Gamma \kappa_N \big(H - H_0\big)^2 \,\mathrm{d}\mu(x);$$

- the Gaussian bending energy,

$$\mathcal{F}_{Helfrich,G}(\Gamma) = \int_\Gamma \kappa_G K \,\mathrm{d}\mu(x)$$

with H_0 the spontaneous curvature, which reflects a possible asymmetry of the capsid. H_0 is usually assumed to be spatially homogeneous. κ_N is the normal bending stiffness and κ_G is the Gaussian bending stiffness. For constant κ_G the Gaussian bending energy is proportional to the Euler characteristic of the capsid (Gauss–Bonnet theorem), and so changes in shape, which preserve the topology, do not contribute to the energy. Hence $\mathcal{F}_{Helfrich,G}$ can be dropped for such cases. In addition we might need to incorporate constraints on volume and/or area. For a review on models based on this energy we refer the reader to [30].

To model the ordering of capsid proteins we follow the approach in [4] and introduce a protein number density ϱ, for which we formulate a Swift–Hohenberg (or phase field crystal) energy $\mathcal{F}_{PFC}$ which reads

$$\mathcal{F}_{PFC}(\varrho,\Gamma) = \int_\Gamma \left(-\|\nabla_\Gamma \varrho\|_\Gamma^2 + \frac{1}{2}(\Delta_\Gamma \varrho)^2 + f(\varrho)\right) \mathrm{d}\mu(x) \tag{1.1}$$

with a potential $f(\varrho) = \frac{1}{2}(1-\varepsilon)\varrho^2 + \frac{1}{4}\varrho^4$ with an adjustable parameter $\varepsilon \in \mathbb{R}$ used to approximate a specific correlation function; see, e.g., [32]. In [4] it has been demonstrated that an H^{-1} gradient flow of this energy converges to a minimal energy configuration which is in correspondence with known results for the classical Thomson problem [33] for optimal ordering of particles on a sphere. In flat space the energy is minimized by a hexagonal structure [14]; however, due to the geometric frustration, which is incorporated through the surface gradient ∇_Γ and the surface Laplacian,

Δ_Γ defects are introduced if the energy is minimized on a curved surface. For typical virus sizes, which are, e.g., for the polyoma virus 72 capsomeres or for the herpes virus 252 units, a minimal energy configuration with 12 isolated disclinations is expected.

The coupling of the macroscopic continuum Helfrich model and the microscopic discrete phase field crystal model comes from the dependency of bending stiffness on the defect structure, which allows a multiscale coupling of the discrete protein arrangements of the capsid and the continuous morphology evolution. It is essentially this interplay between geometry and condensed matter order which provides a fascinating venue for theoretical models; see [6, 34] for two recent reviews. Here for simplicity we consider only the normal bending stiffness κ_N and keep the Gaussian bending stiffness κ_G constant.

The paper is organized as follows. In section 2 we will derive a thermodynamically consistent evolution equation to minimize $\mathcal{F} = \mathcal{F}_{Helfrich} + \mathcal{F}_{PFC}$ with respect to Γ and ϱ. Simplifications of the model according to scale separations are discussed in section 3, and different ways to define the bending rigidity as a function of the defect structure of the protein arrangements are discussed in section 5. In order to numerically solve the derived equations a diffuse interface approximation is used in section 4. In section 6 the adaptive finite element discretization used is described, and implementational details are given. Numerical results are shown in section 7, and conclusions are drawn in section 8.

2. Model derivation. We consider initial data $\Gamma(0) = \Gamma_0$, $\varrho(0,\cdot) = \varrho_0$ and an evolution $(\Gamma(t), \varrho(t))_{t\geq 0}$. We assume that $\Gamma(t)$ is a smoothly evolving family of smooth hypersurfaces with normal velocity $v(t,\cdot)$ that is parametrized over Γ_0,

$$\begin{aligned}\Gamma(t) &= \Phi_t(\Gamma_0),\\ \partial_t \Phi_t(x) &= v(t,x)\nu(t,x),\end{aligned}$$

where $\nu(t,x)$ denotes the outward normal to $\Gamma(t)$ in $x \in \Gamma(t)$. The protein number density $\varrho(t,\cdot)$ is assumed to be a smooth function on $\Gamma(t)$.

We propose evolution equations for ϱ and Φ, which guarantee conservation of protein number density and energy dissipation. Defining the total (material) derivative d_t, we first consider conservation of protein number density ϱ:

$$\frac{d}{dt}\int_{\Gamma(t)} \varrho(x,t)\,\mathrm{d}\mu(x) = \int_{\Gamma(t)} \mathrm{d}_t\varrho(t,x)\,\mathrm{d}\mu(x) + \int_{\Gamma(t)} \varrho(t,x)v(t,x)H(t,x)\,\mathrm{d}\mu(x),$$

where $H(t,\cdot)$ denotes the scalar mean curvature of $\Gamma(t)$, chosen positive if the region enclosed by $\Gamma(t)$ is convex, and where $\mathrm{d}\mu(x)$ denotes integration with respect to the corresponding surface measure. For a detailed definition of the geometric notations we refer the reader to section B.1 in Appendix B. One gets conserved dynamics if one assumes

$$\mathrm{d}_t\varrho = -\varrho v H - \nabla_\Gamma \cdot q \tag{2.1}$$

for a tangential flux q defined by

$$q = -\nabla_\Gamma \partial_\varrho \mathcal{F}, \tag{2.2}$$

where $\partial_\varrho \mathcal{F}$ denotes the variational derivative of $\mathcal{F}$ with respect to ϱ.[1]

[1] ϱ thereby is a protein number density and should not be confused with a protein density as, e.g., considered in [1].

The value of the functional $\mathcal{F}$ changes under the evolution $(\varrho(t,\cdot),\Gamma(t))$, $t\in(0,T)$, according to the equation

$$\mathrm{d}_t\mathcal{F}(\varrho,\Gamma)=\int_\Gamma(\partial_\Phi\mathcal{F}\cdot\mathrm{d}_t\Phi+\partial_\varrho\mathcal{F}\mathrm{d}_t\varrho)\,\mathrm{d}\mu(x). \tag{2.3}$$

By (2.1), (2.2) we compute that

$$\begin{aligned}\mathrm{d}_t\mathcal{F}(\varrho,\Gamma)&=\int_\Gamma\partial_\Phi\mathcal{F}\cdot\mathrm{d}_t\Phi\,\mathrm{d}\mu(x)-\int_\Gamma\partial_\varrho\mathcal{F}(\varrho vH+\nabla_\Gamma\cdot q)\,\mathrm{d}\mu(x)\\&\le\int_\Gamma v\partial_\Phi\mathcal{F}\cdot\nu\,\mathrm{d}\mu(x)-\int_\Gamma\partial_\varrho\mathcal{F}\varrho vH\,\mathrm{d}\mu(x),\end{aligned}$$

where we have used that $\partial_t\Phi$ is normal and partial integration on $\Gamma(t)$. Therefore, dissipative dynamics are obtained by

$$\gamma v=-\partial_\Phi\mathcal{F}\cdot\nu+\varrho\partial_\varrho\mathcal{F}H \tag{2.4}$$

with a kinetic coefficient γ.

To summarize, (2.1), (2.2), (2.4) provide a system of evolution equations which guarantee conservation of protein number density and energy dissipation. The model allows us to simultaneously change the order of proteins and the morphology of the capsid. Thus in principal the formation of new defect structures in the protein arrangement is possible within the interplay of minimizing bending energy and elastic energies of the disclinations. The phase field crystal (PFC) model used here was introduced by Elder et al. [15] and results from phenomenological arguments. However, it can also be derived via a classical dynamic density functional theory from an interatomic potential for the protein interactions; see [3, 16, 32] for a general discussion.

The variational derivatives $\partial_\Phi\mathcal{F}$ and $\partial_\varrho\mathcal{F}$ are computed in Appendix B. The resulting system of partial differential equations forms a highly nonlinear system of a coupled fourth-order equation for the evolution of a surface and a sixth-order equations which has to be solved on the evolving surface. We will not directly use these equations but consider only a special case and prefer a phase field approximation to numerically simulate the evolution equations.

3. Special cases. Instead of solving the full problem (2.1), (2.2), (2.4) we consider the simplification

$$\mathrm{d}_t\varrho=-\varrho vH+\Delta_\Gamma\partial_\varrho\mathcal{F}_{PFC}, \tag{3.1}$$

$$\gamma v=-\partial_\Phi\mathcal{F}_{Helfrich}\cdot\nu+\varrho\partial_\varrho\mathcal{F}H, \tag{3.2}$$

which considers only $\mathcal{F}_{PFC}$ in the first equation and $\mathcal{F}_{Helfrich}$ in the first term of the second equation. The remaining system is no longer thermodynamically consistent. However, besides the achieved simplification, which allows a numerical treatment, there are also physical reasons for these approximations. $\mathcal{F}_{PFC}$ and $\mathcal{F}_{Helfrich}$ consider aspects of the energy on different spatial scales, whereas $\mathcal{F}_{PFC}$ models particle interactions on a molecular scale on a macroscopic surface, and $\mathcal{F}_{Helfrich}$ models this surface. To describe the evolution of the surface, we are thus interested in variations not on a molecular scale but rather only on a macroscopic scale. We thus neglect terms in (3.2) varying on a molecular scale. On the other hand, in (3.1) we are interested in the molecular scale which is primarily determined by $\mathcal{F}_{PFC}$; the dependency

of $\mathcal{F}_{Helfrich}$ on ϱ is due only to the definition of κ_N and thus should not influence the evolution of ϱ.

The protein number density ϱ remains a conserved quantity

$$\frac{d}{dt}\int_{\Gamma(t)} \varrho(x,t)\,\mathrm{d}\mu(x) = \int_{\Gamma(t)} \mathrm{d}_t\varrho + \varrho v H\,\mathrm{d}\mu(x) = \int_{\Gamma(t)} \Delta_\Gamma \partial_\varrho \mathcal{F}_{PFC}\,\mathrm{d}\mu(x) = 0.$$

4. Diffuse interface approximation. We use a diffuse interface approximation and follow the approach in [27] to numerically solve (3.1), (3.2). Therefore we approximate the evolution of the surface that represents the virus capsid by an evolution of smooth phase fields. These take values close to 1 inside the virus and close to 0 outside, with a smooth, but rapid, transition. The corresponding transition layer represents the capsid location. The phase field variables and the governing equations for these fields are defined in a fixed volume domain $\Omega \subset \mathbb{R}^3$ that represents an outer container of the virus. This is a key advantage as the (diffuse) evolution equations now can be numerically solved with standard tools. The main challenge is being computationally efficient, and this requires an adaptive mesh refinement allowing for a fine resolution within the diffuse interface and a coarse resolution away from it.

The phase field approach is based on a diffuse surface area energy for the transition layer. For $\varphi : \Omega \to \mathbb{R}$ representing a phase field variable and a small parameter $\kappa > 0$ such energy is given by

$$\mathcal{A}^\kappa(\varphi) = \int_\Omega \Big(\frac{\kappa}{2}|\nabla\varphi|^2 + \kappa^{-1}G(\varphi)\Big)\,\mathrm{d}x, \tag{4.1}$$

where $G(r)$ is a suitable double-well potential with zeros at $r = 0$ and $r = 1$ that we here choose as $G(r) = 36r^2(1-r)^2$. For energies of order one with respect to the small parameter κ, fields are forced to attain values 0 and 1 in most of the domain Ω, with a transition layer that has finite but small thickness of order κ. By the celebrated Modica–Mortola theorem [25, 24] $\mathcal{A}^\kappa$ approximates the surface area energy in the sense of Gamma-convergence. In particular, sequences with uniformly bounded diffuse area are precompact in L^1, and limit points are characteristic functions of bounded variation.

We derive in the following a diffuse analogue of the sharp interface model. Evolution equations are derived as mass conserving dissipative dynamics. No flux boundary conditions are assumed at $\partial\Omega$. Note that $\partial\Omega$ represents the boundary of an artificial container and that therefore no analogous conditions are present in the sharp interface model.

4.1. Energies. We follow [22] and [2] to approximate the "sharp interface energy" $\mathcal{F}$ by energies for phase fields φ and protein number densities ϱ. We also include penalty terms that account for constraints on the capsid surface area and on the enclosed volume. We assume that the capsid surface is conserved and for all times equals a constant $A_0 > 0$. We relax this condition and introduce in the energy a penalty term

$$\mathcal{P}_A^\kappa(\varphi) = \frac{M_A^\kappa}{2}(\mathcal{A}^\kappa(\varphi) - A_0)^2, \tag{4.2}$$

where M_A^κ is a large positive constant. Similarly we include a volume penalty term

$$\mathcal{P}_V^\kappa(\varphi) = \frac{M_V^\kappa}{2}(V^\kappa(\varphi) - V_0)^2, \quad V^\kappa(\varphi) = \int_\Omega \varphi\,\mathrm{d}x, \tag{4.3}$$

where V_0 is a prescribed value for the enclosed volume and M_V^κ is a large positive constant. The volume functional V^κ is continuous with respect to L^1 convergence and coincides for characteristic functions φ with the volume of the set $\{\varphi = 1\}$.

As a diffuse interface approximation of the Helfrich energy we follow [13] and use

$$\mathcal{F}^\kappa_{Helfrich}[\varrho,\varphi] = \frac{1}{2}\int_\Omega \kappa^{-1}\kappa_N(\varrho)\left(\kappa\Delta\varphi - \kappa^{-1}G'(\varphi) + 6\varphi(1-\varphi)H_0\right)^2 \,\mathrm{d}x, \tag{4.4}$$

where H_0 and κ_N describe the spontaneous curvature and the normal bending stiffness. Here we take κ_N depending on the concentration field ϱ; see below for the precise implementation. Further extensions are possible by allowing the spontaneous curvature to depend on the ordering, e.g., $H_0 = H_0(\varrho)$. We will, however, consider H_0 to be constant. For the special choices $H_0 = 0$ and κ_N constant, (4.4) reduces to the well-known approximation for the Willmore functional proposed by De Giorgi [9]; see also [28].

Next we have to formulate a phase field version of the PFC energy. With this aim we introduce some expressions for a given phase field φ that correspond to the relevant geometric differential operators on a hypersurface Γ. For integration over Γ we choose integration against the surface area density $e_\kappa(\varphi)$,

$$e_\kappa(\varphi) = \frac{\kappa}{2}|\nabla\varphi|^2 + \kappa^{-1}G(\varphi). \tag{4.5}$$

A diffuse version of the surface gradient of a function η is given by

$$\nabla_\kappa\eta \;=\; P_\kappa(\varphi)\nabla\eta, \tag{4.6}$$

where $P_\kappa(\varphi)$ denotes the "tangential projection" (and ν_κ the "normal direction"),

$$P_\kappa(\varphi) \;=\; \mathrm{Id} - \nu_\kappa\otimes\nu_\kappa, \qquad \nu_\kappa \;=\; \frac{\nabla\varphi}{|\nabla\varphi|}. \tag{4.7}$$

Finally, the Laplace–Beltrami operator of a function η is approximated by

$$\Delta_\kappa\eta \;=\; \frac{1}{e_\kappa(\varphi)}\nabla\cdot\left(e_\kappa(\varphi)P_\kappa(\varphi)\nabla\eta\right). \tag{4.8}$$

With this definition we retain analogues of the usual partial integration formulas on surfaces,

$$\int_\Omega \eta\Delta_\kappa\psi\, e_\kappa(\varphi)\,\mathrm{d}x \;=\; -\int_\Omega \nabla_\kappa\eta\cdot\nabla_\kappa\psi\, e_\kappa(\varphi)\,\mathrm{d}x \;=\; \int_\Omega \psi\Delta_\kappa\eta\, e_\kappa(\varphi)\,\mathrm{d}x, \tag{4.9}$$

for all smooth functions η,ψ with compact support in Ω.

With these preparations the natural choice of a diffuse PFC energy is

$$\mathcal{F}^\kappa_{PFC}(\varrho,\varphi) = \int_\Omega \left(f(\varrho) - |\nabla_\kappa\varrho|^2 + \frac{1}{2}(\Delta_\kappa\varrho)^2\right) e_\kappa(\varphi)\,\mathrm{d}x. \tag{4.10}$$

4.2. Variational derivatives. To formulate the diffuse evolution equations corresponding to (3.1), (3.2) we have to compute the derivatives of the diffuse energies chosen above. For the diffuse surface area energy we obtain

$$\partial_\varphi\mathcal{A}^\kappa(\varphi) = -\kappa\Delta\varphi + \kappa^{-1}G'(\varphi). \tag{4.11}$$

In analogy to the formula for the first variation of a surface Γ the expression on the right-hand side is the diffuse interface description of (minus) the scalar mean curvature. For the volume functional we obtain

$$\partial_\varphi V^\kappa(\varphi) = 1. \tag{4.12}$$

Therefore we deduce that

$$\partial_\varphi \mathcal{P}^\kappa_A(\varphi) + \partial_\varphi \mathcal{P}^\kappa_V(\varphi) \;=\; M^\kappa_A(\mathcal{A}^\kappa(\varphi) - A_0)\big(-\kappa\Delta\varphi + \kappa^{-1}G'(\varphi)\big) + M^\kappa_V(V(\varphi) - V_0). \tag{4.13}$$

For the variational derivative of the diffuse Helfrich energy with respect to the phase field variable we obtain

$$\partial_\varphi \mathcal{F}^\kappa_{Helfrich}(\varrho,\varphi) = \Delta\omega - \kappa^{-2}G''(\varphi)\omega + \kappa^{-1}H_0 6(1-2\varphi)\omega,$$

with

$$\omega = \kappa_N(\varrho)\left(\kappa\Delta\varphi - \kappa^{-1}G'(\varphi) + 6\varphi(1-\varphi)H_0\right).$$

To obtain the derivative of the diffuse PFC energy with respect to ϱ we recall that for a smooth variation field η we have

$$\int_\Omega \partial_\varrho \mathcal{F}^\kappa_{PFC}(\varrho,\varphi)\cdot\eta e_\kappa(\varphi)\,dx = \frac{d}{ds}\Big|_{s=0}\mathcal{F}^\kappa_{PFC}(\varrho+s\eta,\varphi).$$

We compute the right-hand side and start with the first term in the energy and obtain that

$$\frac{d}{ds}\Big|_{s=0}\int_\Omega f(\varrho+s\eta)\,e_\kappa(\varphi)\,dx = \int_\Omega f'(\varrho)\eta e_\kappa(\varphi)\,dx.$$

For the second term we obtain by the partial integration formula (4.9)

$$\frac{d}{ds}\Big|_{s=0}\int_\Omega |\nabla_\kappa(\varrho+s\eta)|^2\,e_\kappa(\varphi)\,dx = 2\int_\Omega \nabla_\kappa\varrho\cdot\nabla_\kappa\eta\,e_\kappa(\varphi)\,\mathrm{d}x = -2\int_\Omega \Delta_\kappa\varrho\eta\,e_\kappa(\varphi)\;\mathrm{d}x.$$

Finally, for the last term in the energy we similarly derive

$$\frac{d}{ds}\Big|_{s=0}\frac{1}{2}\int_\Omega(\Delta_\kappa(\varrho+s\eta))^2\,e_\kappa(\varphi)\,\mathrm{d}x = \int_\Omega \Delta_\kappa\varrho\Delta_\kappa\eta e_\kappa(\varphi)\,\mathrm{d}x = \int_\Omega \eta(\Delta_\kappa)^2\varrho e_\kappa(\varphi)\,\mathrm{d}x.$$

From this, we obtain the complete result

$$\partial_\varrho\mathcal{F}^\kappa_{PFC}(\varrho,\varphi) = f'(\varrho) + 2\Delta_\kappa\varrho + (\Delta_\kappa)^2\varrho.$$

4.3. Diffuse evolution equations. We derive a system of evolution equations for phase fields φ and protein number densities ϱ that corresponds to the sharp interface equations (3.1), (3.2). Again we start with mass conservation of the protein number densities. Assuming a no-flux boundary condition for φ, we compute

$$\frac{d}{dt}\int_\Omega \varrho\,e_\kappa\,dx \;=\; \int_\Omega \partial_t\varrho e_\kappa - \kappa\nabla\varrho\cdot\nabla\varphi\partial_t\varphi + (-\kappa\Delta\varphi + \kappa^{-1}G'(\varphi))\varrho\partial_t\varphi\,dx. \tag{4.14}$$

We choose μ in analogy to (3.1) as

$$\mu = \partial_\varrho\mathcal{F}^\kappa_{PFC}(\varrho,\varphi) \tag{4.15}$$

and impose a no-flux boundary condition for μ. From (4.14) mass conservation for ϱ follows if we prescribe that

$$\partial_t \varrho e_\kappa - \kappa \nabla \varrho \cdot \nabla \varphi \partial_t \varphi = (\kappa \Delta \varphi - \kappa^{-1} G'(\varphi)) \varrho \partial_t \varphi + \nabla \cdot \big(e_\kappa P_\kappa(\varphi) \nabla \mu \big). \tag{4.16}$$

Here we have used that $P_\kappa(\varphi)\nabla\mu \cdot \nu = 0$ on $\partial\Omega$ follows by the no-flux boundary condition for φ, μ. The dynamics (4.16) now corresponds to (3.1) as the expressions on the left-hand side both describe the total derivative.

We translate the surface evolution equation (3.2) in a similar way, include the variational derivatives of the penalty terms, and obtain the evolution equation

$$\gamma \kappa \partial_t \varphi = -\partial_\varphi \mathcal{F}^\kappa_{Helfrich} - \partial_\varphi \mathcal{P}^\kappa_A(\varphi) - \partial_\varphi \mathcal{P}^\kappa_V(\varphi) - \varrho\mu(\kappa\Delta\varphi - \kappa^{-1} G'(\varphi)) \tag{4.17}$$

with μ the chemical potential defined through (4.15).

The resulting system of equations for ϱ and φ is of sixth and fourth order, respectively. We expect that the protein number density ϱ and the chemical potential μ are in highest order constant in the direction normal to the transition layer of φ; see [27] for an asymptotic analysis of a similar (yet simpler) case. In this case we can neglect the projection map P_κ and can further reduce (4.16), (4.17). Furthermore we assume $H_0 = 0$. When we write the equations as systems of second-order equations, the model to be solved reads as follows: Find φ, ω, ϱ, μ, and ν such that

$$\begin{aligned} \gamma\kappa\partial_t\varphi &= -(\Delta\omega + \kappa^{-2} G''(\varphi)\omega) - \varrho\mu \frac{\omega}{\kappa_N(\varrho)} \\ &\quad + M^\kappa_A(\mathcal{A}^\kappa(\varphi) - A_0)\frac{\omega}{\kappa_N(\varrho)} + M^\kappa_V(V^\kappa(\varphi) - V_0), \end{aligned} \tag{4.18}$$

$$\omega = \kappa_N(\varrho)(\kappa\Delta\varphi - \kappa^{-1} G'(\varphi)), \tag{4.19}$$

$$e_\kappa \partial_t \varrho = (\kappa \nabla \cdot (\varrho \nabla \varphi) - \kappa^{-1} G'(\varphi)\varrho)\partial_t\varphi + \nabla \cdot (e_\kappa \nabla \mu), \tag{4.20}$$

$$e_\kappa \mu = e_\kappa f'(\varrho) + 2 e_\kappa \nu + \nabla \cdot (e_\kappa \nabla \nu), \tag{4.21}$$

$$e_\kappa \nu = \nabla \cdot (e_\kappa \nabla \varrho), \tag{4.22}$$

with appropriate initial conditions for φ and ϱ and zero flux boundary conditions for all variables.

5. Definition of the bending stiffness. We introduce two ways of defining the particle dependent bending stiffness. In the first approach, which we will refer to as discrete defect localization (DDL), we divide the set of particles into defects and nondefects. Then we set the bending stiffness to a certain value in the defects, to a different value in the nondefects, and interpolate in between. In the second approach, which will be called variational bending stiffness (VBS), we will use the variational derivative $\partial_\varphi \mathcal{F}_{PFC}(\varrho, \Gamma)$ to define the bending stiffness. Both approaches are phenomenologically motivated without a rigorous justification.

5.1. Discrete defect localization. To make the normal bending stiffness dependent on the occurrence of defects, we first need to determine the defects. This is done in four steps.

1. Calculate a restriction of ϱ to the interface:

$$\tilde{\varrho} = e_\kappa \cdot \varrho.$$

2. Locate the positions p_i of isolated maxima of $\tilde{\varrho}$ passing a threshold: $\tilde{\varrho}(p_i) > 0$. Thereby i is an index labeling the isolated maxima (positions of proteins) from 1 to N, where N is the number of maxima found.
3. Count the number of neighbors n_i of the protein at position p_i. We use the Euclidean distance and set

$$n_i = \sum_{j \neq i : ||p_i - p_j||_2 < 1.5a} 1,$$

where $a = \frac{4}{\sqrt{3}}\pi$ is the default distance of particles in the PFC model in a perfect hexagonal structure. Of course, the Euclidean distance is a good approximation only for small curvature values. It worked very well in all of our examples.
4. We set the normal bending stiffness

$$\kappa_N(x) = M_N \min\Big\{ \min_{i : n_i \neq 6} |x - p_i|, a \Big\}$$

with a constant scaling factor M_N.

Note that this gives $\kappa_N = 0$ in the defects and $\kappa_N = M_N a$ away from the defects, with a linear transition in between, which will allow for the desired faceting of the structure. As $\kappa_N = 0$ results in a degeneracy of the problem, we replace κ_N by $\kappa_N + \delta_{\kappa_N}$ in the simulations, with $\delta_{\kappa_n} = 10^{-4}$.

Besides the limitations corresponding to large curvatures, wrong classification of neighbors may also occur if the particle distribution is not equilibrated using the DDL approach.

5.2. Variational bending stiffness. As an alternative to the DDL method we might describe the ordered arrangement in terms of the interactions of its defects, which leads to a more mesoscopic approach. Thereby the energetics of the defects provide a useful starting point for deriving inhomogeneities in the normal bending stiffness. On a spherical topology defects are necessarily introduced into the lattice structure. The number of disclinations for a spherical topology has to be at least 12. Their repulsive interaction will favor an arrangement which maximizes their separation leading to a configuration with icosahedral symmetry. In [21] it was shown that the competition of the strain associated with the disclinations and the bending energy leads to a buckling transition from a smooth round shape to a sharply faceted shape with increasing size. We demonstrate the increase of the strain energy in the disclinations with increasing size by considering capsids with icosahedral symmetry. An icosahedron is build by 20 identically curved, equilateral triangles. Therefore it is sufficient to consider only one of these triangles. In Figure 5.1 we computed equilibrium particle arrangements on one of these triangles for increasing R and thus increasing number of particles N. Note that N denotes the total number of particles on the whole sphere.

A comparison of the energy density in pentamers and hexamers for these configurations is shown in Figure 5.2 indicating an increase in the elastic energy in the pentamers.

Using the differences in the energy density in $\mathcal{F}_{PFC}$ between pentamers and hexamers to define an effective dependency of the normal bending rigidity on the defect structure allows us to circumvent to DDL approach described above. Due to an increase in the difference between the energy density in pentamers and hexamers for

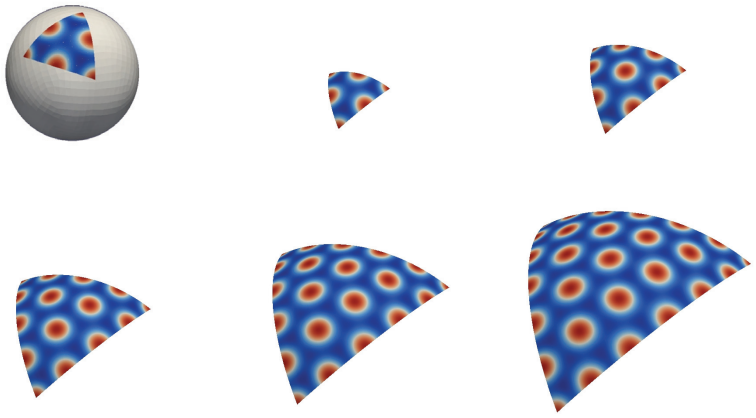

FIG. 5.1. *Icosahedral arrangement on a sphere with* $N = 42$, 92, 162, 252, *and* 362 *(from top left to bottom right). Shown is one portion of the sphere, with pentamers arranged in the corners. The radius* R *is varied to realize the different particle numbers by keeping the physical parameters in* $\mathcal{F}_{PFC}$ *fixed at* $\epsilon = 0.4$ *and* $\bar{\varrho} = -0.3$.

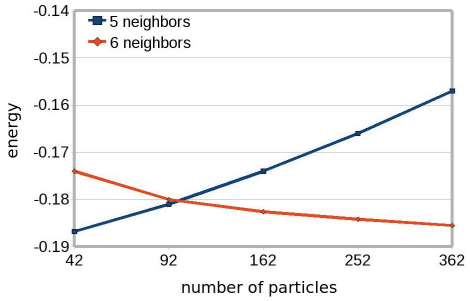

FIG. 5.2. *Energy density* $f(\varrho) - |\nabla_\kappa \varrho|^2 + \frac{1}{2}(\Delta_\kappa \varrho)^2$ *of* $\mathcal{F}_{PFC}$ *in the center of the pentamers and hexamers as a function of* N*, corresponding to the arrangements shown in Figure* 5.1. *Shown is the averaged density over all pentamers and hexamers, respectively. The values of the individual pentamers and hexamers are almost identical.*

increasing radius R, also the strength of the anisotropy in the normal bending rigidity can be modeled as a function of R. This allows us to tune the asphericality of the capsid as a function of R. But, as the difference in the energy density becomes significant only for large particle numbers, this approach requires us to solve much larger systems, which can no longer be handled without massively parallel computing.

Hence, instead of using the energy density, we will use the variation of $\mathcal{F}_{PFC}(\varrho, \Gamma)$ with respect to Γ. In fact, this is a natural way to define the evolution of Γ so that the energy is minimized. As shown in Appendix B the computation of $\partial_\Phi \mathcal{F}_{PFC}(\varrho, \Gamma)$ leads to rather complicated terms. Similarly the variational φ-derivative of the diffuse approximation $\mathcal{F}^\kappa_{PFC}(\varrho, \varphi)$ is rather complex. However, assuming that equipartition of energy

$$\frac{\kappa}{2}|\nabla\varphi|^2 \;=\; \frac{1}{\kappa}G(\varphi)$$

holds to lowest order in κ and, moreover, that ϱ and $\Delta_\kappa \varrho$ are to lowest order constant in the normal direction (cf. [27]), we can approximate (see Appendix A)

(5.1)
$$\partial_\varphi \mathcal{F}^\kappa_{PFC}(\varrho,\varphi) \approx w_\kappa g + 2\kappa \nabla\varrho \cdot D^2\varphi \nabla\varrho - w_\kappa \nabla(\Delta_\kappa\varrho)\cdot\nabla\varrho - 2\kappa\nabla(\Delta_\kappa\varrho)\cdot D^2\varphi\nabla\varrho,$$

where

$$w_\kappa = -\kappa\Delta\varphi + \frac{1}{\kappa}G'(\varphi), \quad g = f(\varrho) - |\nabla\varrho|^2 - \frac{1}{2}(\Delta_\kappa\varrho)^2.$$

The corresponding variational derivative of the sharp interface analogues (see Appendix B) formally agrees with this approximation, in the sense that

$$\delta_\varphi \mathcal{F}^\kappa_{PFC}(\varrho,\varphi)(-\nabla\varphi\cdot\eta) + \delta_\varrho \mathcal{F}^\kappa_{PFC}(\varrho,\varphi)(-\nabla\varrho\cdot\eta) \approx \delta_\Phi \mathcal{F}_{PFC}(\varrho,\Gamma)(\eta)$$

for smooth variation fields $\eta \in C^2_c(\Omega,\mathbb{R}^n)$. Note that in the diffuse case both variational derivatives appear since we have moved the concentration field with the variation of the surface when computing the sharp interface variational derivatives. Furthermore, the inner variation in the direction of η that we have used in the sharp interface case translates into variations of the diffuse variables φ, ϱ in the direction of $-\nabla\varphi\cdot\eta$ and $-\nabla\varrho\cdot\eta$, respectively.

Note that the usual energy minimizing evolution laws

$$\partial_t\varphi = -\partial_\varphi \mathcal{F}^\kappa_{PFC}(\varrho,\varphi)$$

and

$$\partial_t\varphi = \Delta\left(\partial_\varphi \mathcal{F}^\kappa_{PFC}(\varrho,\varphi)\right)$$

result in an anisotropic Allen–Cahn and Cahn–Hilliard equation, respectively. Still, these equations vary on the spatial scale of the proteins, which is not desired. And, even worse, the equations are ill-posed since g can be (and in fact is) negative in some areas. Hence one cannot directly use the evolution laws, but the derivation suggests that $\partial_\varphi \mathcal{F}^\kappa_{PFC}(\varrho,\varphi)$ describes the anisotropy and can therefore be used to design the bending stiffness. Since we do not want to consider variations of $\partial_\varphi \mathcal{F}^\kappa_{PFC}(\varrho,\varphi)$ on spacial scales smaller than the particle distance, we only evaluate $\partial_\varphi \mathcal{F}^\kappa_{PFC}(\varrho,\varphi)$ in the particle position, and thus at the discrete maxima of ϱ. In these locations $\nabla\varrho$ vanishes and the approximation to $\partial_\varphi \mathcal{F}^\kappa_{PFC}(\varrho,\varphi)$ simplifies to $w_\kappa g$. Hence the information about the anisotropy is contained in g.

Figure 5.3 shows a sphere colored with the value of g at the position of the closest neighboring particle. We see that g is also well-suited for use as an indicator for the defects since it has significantly distinct values in the pentamers and in the hexamers. This indicator is quite natural and does not put any restrictions on the curvature as the DDL approach does.

We take a closer look at the dependence of g on the number of particles N. Again we use the equilibrium distribution on the curved triangles building an icosahedron (see Figure 5.1). Figure 5.4 shows g for $N = 42, 92, 162, 252, 362$. As expected the anisotropy, that is, the difference in g between pentamers and hexamers, increases with N. Therefore using g for the bending stiffness should give a reasonable model

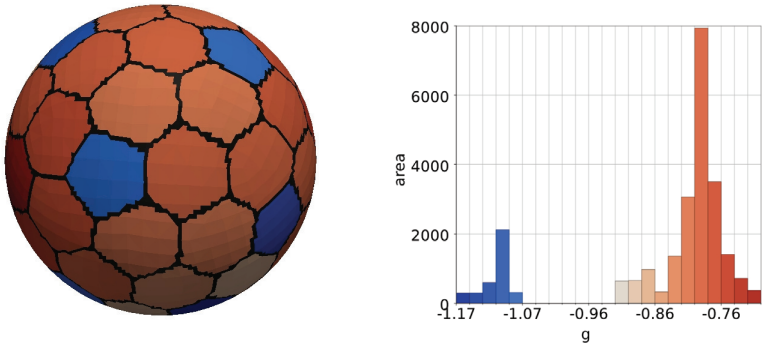

FIG. 5.3. *Left: A sphere with 73 particles colored with the function g evaluated at the next neighboring particle position. The black lines are added to enhance the edges for visibility. Right: The corresponding histogram showing distinct values for pentamers and hexamers.*

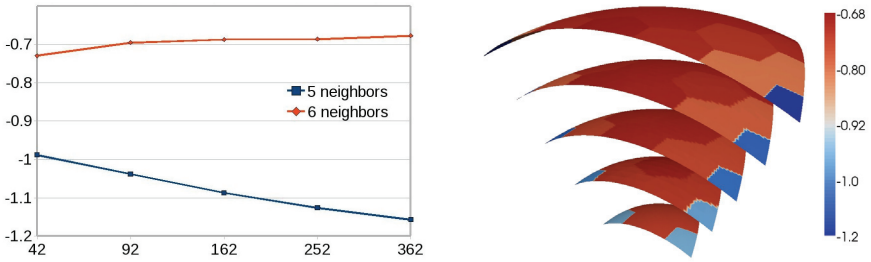

FIG. 5.4. *The value of* $g = f(\varrho) - |\nabla \varrho|^2 - \frac{1}{2}(\Delta_\kappa \varrho)^2$ *in the center of the pentamers and hexamers as a function of* N*, corresponding to the arrangements shown in Figure* 5.1.

and should yield more faceted shapes for higher particle numbers, which reflects the experimentally observed increase in asphericality of viral capsids for increasing N.

To build the bending stiffness κ_N we will, as before, evaluate g only at the particle positions p_i. Therefore we interpolate in between using radial basis functions. We use the interpolant

$$\tilde{g}(x) := \sum_i w_i e^{-\beta ||x-p_i||^2},$$

where the weights w_i are calculated by requiring $\tilde{g}(p_i) = g(p_i)$, and β is adjusted to define the shape of the radial basis functions. To avoid negative values we finally set the bending stiffness

$$\kappa_N(x) = M_N \left(g(x) - \min\{g(x) : x \in \Omega\} \right), \tag{5.2}$$

with the scaling factor M_N. Again we replace κ_N by $\kappa_N + \delta_{\kappa_N}$ in the numerical approach.

6. Numerical approach. We will solve (4.18)–(4.22) using linear finite elements. To discretize in time we decompose the time interval [0,T] into $M \in \mathbb{N}$ equidistant intervals of mesh size $\tau := T/M$. We define the discrete time derivative

$D_t v^{m+1} := (v^{m+1} - v^m)/\tau$, where the superscripts denote the time iteration. We use a semi-implicit Euler scheme, where we keep as many terms implicit as possible. Hence, in every time step the following coupled system has to be solved:

$$\begin{aligned}\gamma\kappa D_t\varphi^{m+1} &= -(\Delta\omega^{m+1} + \kappa^{-2}G''(\varphi^m)\omega^{m+1}) - \varrho^m\mu^m\frac{\omega^{m+1}}{\kappa_N(\varrho^m)}\\ &\quad + M_A^\kappa(\mathcal{A}^\kappa(\varphi^m) - A_0)\frac{\omega^{m+1}}{\kappa_N(\varrho^m)} + M_V^\kappa(V^\kappa(\varphi^m) - V_0), \qquad (6.1)\\ \omega^{m+1} &= \kappa_N(\varrho^m)(\kappa\Delta\varphi^{m+1} - \kappa^{-1}G'(\varphi^{m+1})), \qquad (6.2)\\ e_\kappa^m D_t\varrho^{m+1} &= (\kappa\nabla\cdot(\varrho^m\nabla\varphi^m) - \kappa^{-1}G'(\varphi^m)\varrho^m)D_t\varphi^{m+1} + \nabla\cdot(e_\kappa^m\nabla\mu^{m+1}), \qquad (6.3)\\ e_\kappa^m\mu^{m+1} &= e_\kappa^m f'(\varrho^{m+1}) + 2e_\kappa^m\nu^{m+1} + \nabla\cdot(e_\kappa^m\nabla\nu^{m+1}), \qquad (6.4)\\ e_\kappa^m\nu^{m+1} &= \nabla\cdot(e_\kappa^m\nabla\varrho^{m+1}). \qquad (6.5)\end{aligned}$$

The potentials $f'(\varrho)$ and $G'(\varphi)$ are linearized by a Taylor expansion, dropping terms of order two and higher so that the equations are linear at the implicit time step. We iterate only once in each time step. The same discretization approach has already been used for (6.3)–(6.5) for stationary surfaces ($D_t\varphi^{m+1} = 0$) in [3]. The discretization for (6.1), (6.2) is taken from [22], now with the protein number density instead of an order parameter. Results are not available for consistency and stability in the case when both approaches are combined in the described way.

For the spatial derivatives we use the adaptive finite element toolbox AMDiS [36] with linear test functions for all variables. The linear system is solved using BiCGStab(ell). To ensure the well-posedness of the equations, e_κ is replaced by $e_\kappa + \xi$ with a small parameter $\xi = 10^{-6}$.

Adaptive meshes are indispensable for providing a high spatial resolution along the interface. For local mesh adaptation, we use an L^2-like error indicator based on a jump residual (see, e.g., [35, 36]) for φ to maintain approximately five grid points across the transition layers.

7. Numerical results. We do simulations with both models for the bending stiffness, that is, DDL and VBS. All computations are carried out in the following way.

The initial condition for φ is prescribed by $\varphi = 0.5\big(1 + \tanh(d/\sqrt{2}\kappa)\big)$ for a given signed distance function d. First, we keep this φ fixed and solve only the PFC equations (6.3)–(6.5). We use a uniform distributed random perturbation in $[-0.4, -0.2]$ as initial value for ϱ. We stop the pure PFC system when a steady state is reached, that is, when an equilibrium distribution of particles on the surfaces is reached. Then in a second step we allow the interface to move. Therefore we solve the complete coupled system (6.1)–(6.5), taking ϱ from the previous calculation as initial value.

In all simulations we neglect spontaneous curvature H_0 in the normal bending energy. The incorporation of this term is not an issue in the computational approach but might be of relevance if the viral building blocks had a pronounced conical shape [7]. Furthermore we set the kinetic coefficient $\gamma = 1$.

First, we present results of the DDL. Figure 7.1 shows an example for the evolution of a sphere towards the faceted icosahedral shape. Here we use $\Omega = [-15, 15]^3$ and a radius of 11.5 (i.e., $d = 11.5 - |x|$). The sphere is covered with 32 particles which yield 12 disclinations. Further parameters are $\kappa = 0.6$, $M_N = 120$, $M_A^\kappa = 15.0$, $M_V^\kappa = 0$, $T = 1$, $\tau = 0.001$, and $\epsilon = 0.4$. For A_0 we use the value of $\mathcal{A}^\kappa(\varphi)$ at time $t = 0$.

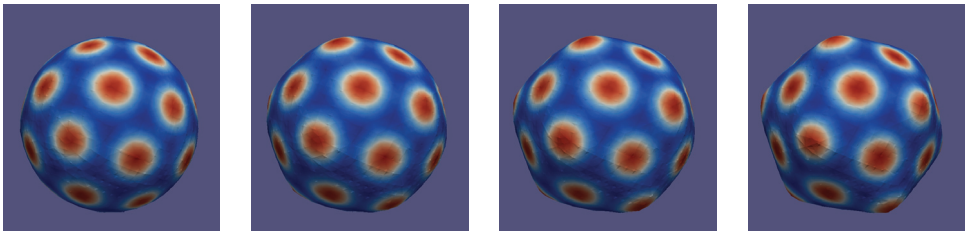

FIG. 7.1. *Evolution of a sphere covered with* 32 *proteins towards an icosahedral shape. The times shown are* $t = 0, 0.01, 0.02, 1.0$.

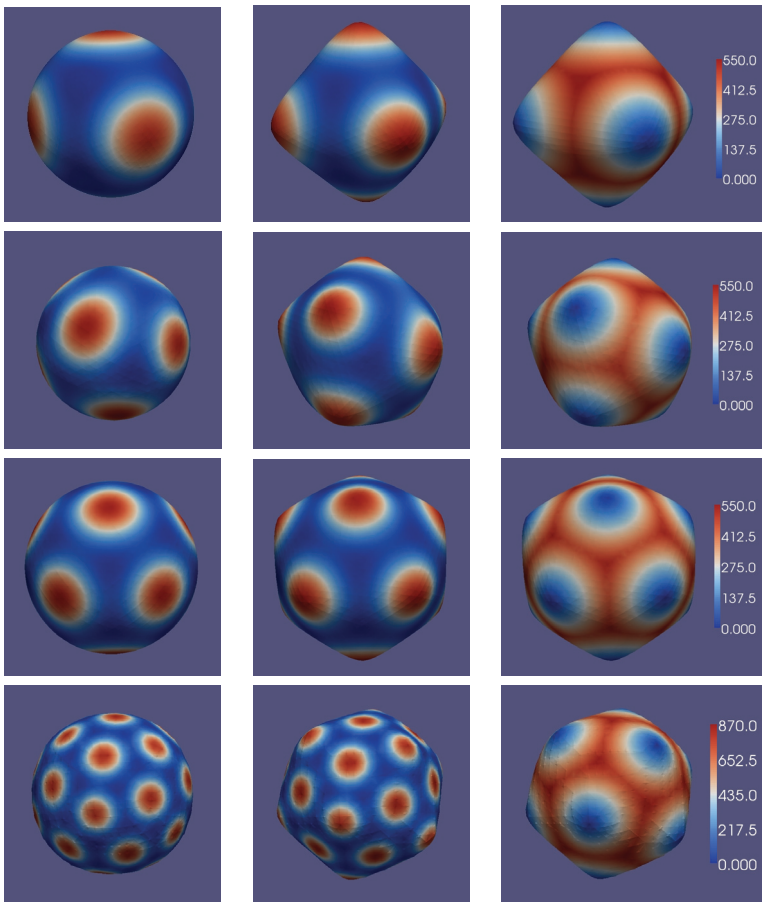

FIG. 7.2. *Spheres with* 6, 9, 12, *and* 32 *proteins. Initial condition (left), final state (middle), and bending stiffness at final time (right).*

All parameters are chosen after extensive numerical experiments, e.g., M_A^κ such that the area is conserved.

We also do simulations for smaller spheres of radius 5.0, 6.0, and 7.0 yielding 6, 9, and 12 proteins. In the DDL approach every particle is a disclination and the sphere buckles in each of them. Figure 7.2 shows initial condition, steady state, and the bending stiffness on the surface.

The last DDL example shows the evolution of a sphere with radius 40 covered with 344 particles. Here, particles with 5, 6, and 7 neighbors occur. The arrangement of particles is irregular and leads to a nonicosahedral shape. Figure 7.3 shows initial condition, steady state, and the bending stiffness on the surface. One can also see chains of particles with alternately five and seven neighbors, so-called grain boundary scars, which have been discussed for droplets covered by colloidal particles [5]. For this simulation we take $\Omega = [-60, 60]^3$, $\tau = 0.01$, $M_N = 1200$, $M_A^\kappa = 3$, and further parameters as before.

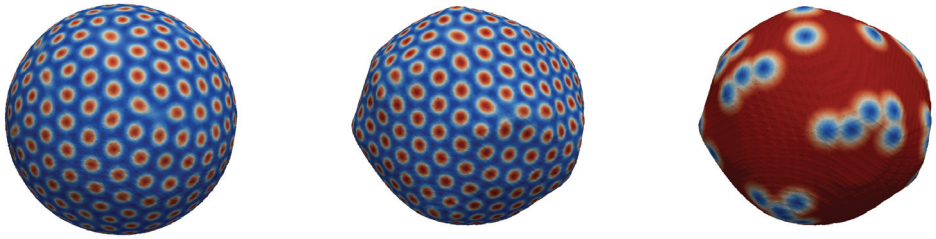

FIG. 7.3. *Sphere covered with* 344 *proteins. Initial condition (left), final state (middle), and bending stiffness at final time (right).*

Next, we do simulations with the VBS model. We start with a sphere of radius 6.0 which yields nine particles. Three of them have only four neighbors; the remaining six particles have five neighbors. Figure 7.4 shows a time evolution of the morphology. In contrast to the DDL approach this configuration leads to a quasi-triangular shape, where the three particles with only four neighbors occupy the edges. The parameters are chosen as $\beta = 0.06$, $\tau = 0.1$, $T = 30$, $M_N = 3$, $M_A^\kappa = 1$.

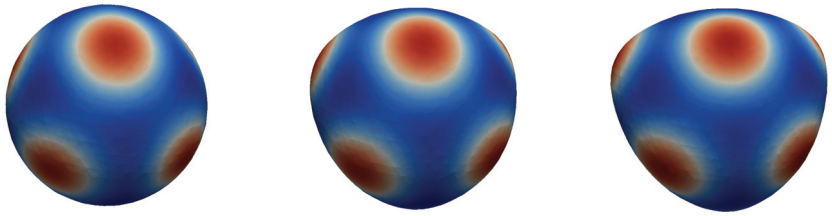

FIG. 7.4. *A sphere covered with* 9 *proteins evolves to a triangular-like shape. Shown times are* $t = 0, 5, 30$.

In order to validate the approach further we compute the PFC surface energy. Figure 7.5 shows the evolution over time and indicates a decrease in the PFC energy. Thus even without a direct minimization of the PFC energy the definition of the bending stiffness already allows for morphology changes, which lead to a decreasing PFC energy. This clearly demonstrates the validity of our effective multiscale approach for surface evolution.

Finally, we demonstrate evolutions of bigger spheres with 12, 32, and 93 particles, respectively. Figure 7.6 shows the morphology at final time. The parameters are as before, except for $\beta = 0.03$ and $M_N = 300$, which speed up the evolution.

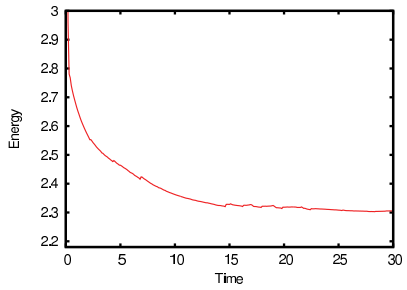

FIG. 7.5. *PFC surface energy, $\mathcal{F}^{\kappa}_{PFC}(\varrho,\varphi)$ over time. The occasional increase of the energy corresponds to protein rearrangements as a result of changes in the surface morphology. The overall energy is decreasing.*

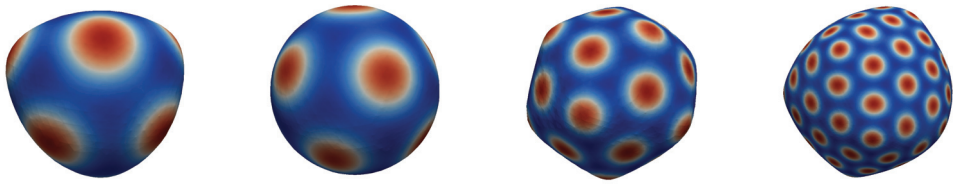

FIG. 7.6. *Final shape of surfaces with* 9, 12, 32, *and* 93 *proteins.*

8. Discussion. The different shapes of spherical-like viral capsids which change from spherical to faceted can be explained by a buckling transition resulting from a balance between the stretching energy associated with the pentamers in capsomer lattices and the bending elasticity of the viral capsid [21]. We model this within a continuum multiscale approach allowing for reordering of proteins and shape changes simultaneously. In [20] a similar approach is used to study crystalline order on flexible surfaces within a lattice model. The interplay between formation of grain boundary scars to minimize the stretching energy associated with disclinations on rigid surfaces and the possibility of minimizing the energy by buckling is investigated for surfaces with spherical topology. In [20] it is computationally found that the buckling transition shifts to higher values of the Föppl–von Karman number γ due to the presence of scars. Due to the high computational cost of the diffuse domain approach used, we could not confirm these results. But we also observe the formation of grain boundary scars for the largest considered example. However, grain boundary scars have not been observed on viruses as they are too small in size. But the coupling between in-plane order and the geometry with the possibility of changing local arrangements and the shape of the surface simultaneously might play a crucial role in other structures, e.g., in membranes [23] with lipids playing the role of interacting particles. However, due to the fluid-like nature of membranes the crystalline order is assumed to be of relevance only within the gel phase.

Polymer vesicles in which the lipids are replaced by amphiphilic block copolymers are of even more importance, as they are much more stable and are expected to have wider applications in materials science and biotechnology. There is a close connection between the morphology of polymer vesicles and the chemical structure of the constituent block copolymers [11]. The shape anisotropy can thereby be introduced by crystalline [10] and liquid crystalline [38] structures. Within a modeling approach

this has been considered in [19]. Other applications consider crystalline monolayers of colloids confined on curved interfaces between immiscible fluids [12, 5, 31], which has been considered within a similar continuum approach in [2]. In all of these applications the number of interacting particles is much larger and within the regime of the formation of grain boundary scars. Furthermore one advantage of our approach becomes relevant, as nonspherical shapes or topological changes might occur. However, in the latter case the Gaussian curvature term in the energy can no longer be neglected.

In our approach we use the crystalline order, or to be more precise, the defects within the crystalline structure in the microscopic model, to define an effective anisotropy in the macroscopic description of the geometry. The normal bending rigidity κ_N becomes a function of the underlying defect structure and thus incorporates the defects' stretching energy.

The computational approach is based on a diffuse interface approximation which allows us to formulate the problem as a system of partial differential equations within a three-dimensional domain, and thus allows its solution using only standard tools. To be computationally efficient, adaptive refinement is required along the diffuse interface. The approach is not restricted to spherical-like shapes but can be used for arbitrary shapes.

Appendix A. Variational φ-derivative of the diffuse PFC energy. In this section we compute the variational derivative $\delta_\varphi \mathcal{F}^\kappa_{PFC}|_{(\varrho,\varphi)}(\eta)$ of the diffuse PFC energy at (ϱ, φ) with respect to the variable φ in the direction of a smooth variation field $\eta \in C_c^\infty(\Omega)$, and we justify the approximation (5.1) that was used in the variational approach to define a reasonable bending stiffness. We first collect some derivatives that we will need in our computations.

For the variational derivative of the diffuse surface energy we obtain

$$\delta_\varphi e_\kappa|_\varphi(\eta) \;=\; \kappa\nabla\varphi\cdot\nabla\eta + \frac{1}{\kappa}G'(\varphi)\eta \;=\; \nabla\cdot(\kappa\eta\nabla\varphi) + w_\kappa(\varphi)\eta, \tag{A.1}$$

with the diffuse scalar mean curvature

$$w_\kappa(\varphi) \;=\; -\kappa\Delta\varphi + \frac{1}{\kappa}G'(\varphi).$$

The inner normal to the level sets of φ is

$$\nu \;=\; \nu(\varphi) \;:=\; \frac{\nabla\varphi}{|\nabla\varphi|}.$$

We compute that

$$\delta_\varphi \nu|_\varphi(\eta) \;=\; \frac{1}{|\nabla\varphi|}P(\varphi)\nabla\eta, \tag{A.2}$$

with the tangential projection

$$P \;=\; P(\varphi) \;=\; \mathrm{Id} - \nu(\varphi)\otimes\nu(\varphi).$$

Next we obtain for the variational derivative of this projection

$$\delta_\varphi P|_\varphi(\eta) \;=\; -\frac{1}{|\nabla\varphi|}\Big(P\nabla\eta\nu^T + \nu\nabla\eta^T P\Big). \tag{A.3}$$

Furthermore we need several spatial derivatives that we collect for further use. First,

$$\nabla e_\kappa \;=\; \kappa D^2\varphi\nabla\varphi + \frac{1}{\kappa}G'(\varphi)\nabla\varphi. \tag{A.4}$$

For $r > 0$ we have

$$D\left(\frac{\nabla\varphi}{|\nabla\varphi|^r}\right) \;=\; \frac{1}{|\nabla\varphi|^r}\Big(\mathrm{Id} - r\nu\nu^T\Big)D^2\varphi. \tag{A.5}$$

For the projection we deduce

$$\partial_k P_{ij} \;=\; -\frac{1}{|\nabla\varphi|}P_{il}\partial^2_{lk}\varphi\,\nu_j - \nu_i\frac{1}{|\nabla\varphi|}P_{jl}\partial^2_{lk}\varphi, \tag{A.6}$$

$$\nabla\cdot P(\varphi) \;=\; -\frac{1}{|\nabla\varphi|}\Big(\mathrm{Id} - 2\nu\nu^T\Big)D^2\varphi\nu - \frac{1}{|\nabla\varphi|}\Delta\varphi\nu. \tag{A.7}$$

We now compute the variational derivative of the second-order term in the PFC energy:

$$\delta_\varphi\left(\int_\Omega \frac{1}{2}\big(\Delta_\kappa\varrho\big)^2 e_\kappa\,dx\right)(\eta) = \int_\Omega \frac{1}{2}\big(\Delta_\kappa\varrho\big)^2\delta_\varphi e_\kappa(\eta) + \big(\Delta_\kappa\varrho\big)\delta_\varphi\big(\Delta_\kappa\varrho\big)(\eta)e_\kappa\,dx \;=:\; I. \tag{A.8}$$

We obtain

$$\begin{aligned}\delta_\varphi\big(\Delta_\kappa\varrho\big)(\eta) &= \delta_\varphi\left(\frac{1}{e_\kappa}\nabla\cdot(e_\kappa P\nabla\varrho)\right)(\eta)\\ &= -\frac{1}{e_\kappa}\delta_\varphi e_\kappa(\eta)\Delta_\kappa\varrho + \frac{1}{e_\kappa}\nabla\cdot\big(\delta_\varphi e_\kappa(\eta)P\nabla\varrho\big) + \frac{1}{e_\kappa}\nabla\cdot\big(e_\kappa\delta_\varphi P(\eta)\nabla\varrho\big),\end{aligned}$$

and hence

$$\begin{aligned}I \;=\; I_1 + I_2 + I_3 \;:=\; \int_\Omega -\frac{1}{2}\big(\Delta_\kappa\varrho\big)^2\delta_\varphi e_\kappa(\eta)\,dx + \int_\Omega \big(\Delta_\kappa\varrho\big)\nabla\cdot\big(\delta_\varphi e_\kappa(\eta)P\nabla\varrho\big)\,dx\\ + \int_\Omega \big(\Delta_\kappa\varrho\big)\nabla\cdot\big(e_\kappa\delta_\varphi P(\eta)\nabla\varrho\big)\,dx.\end{aligned}$$

Using (A.1), we have

$$\begin{aligned}I_1 &= \int_\Omega -\frac{1}{2}\big(\Delta_\kappa\varrho\big)^2\Big(\nabla\cdot(\kappa\eta\nabla\varphi) + w_\kappa(\varphi)\eta\Big)\,dx\\ &= \int_\Omega\left[\big(\Delta_\kappa\varrho\big)\nabla\big(\Delta_\kappa\varrho\big)\cdot\kappa\nabla\varphi - \frac{1}{2}\big(\Delta_\kappa\varrho\big)^2 w_\kappa\right]\eta\,dx\end{aligned} \tag{A.9}$$

and

(A.10)
$$\begin{aligned} I_2 &= -\int_\Omega P\nabla\big(\Delta_\kappa\varrho\big)\cdot\nabla\varrho\,\big(\nabla\cdot(\kappa\eta\nabla\varphi)+w_\kappa\eta\big)\,dx \\ &= \int_\Omega \nabla\Big(P\nabla\big(\Delta_\kappa\varrho\big)\cdot\nabla\varrho\Big)\cdot\kappa\nabla\varphi\,\eta\,dx - \int_\Omega P\nabla\big(\Delta_\kappa\varrho\big)\cdot\nabla\varrho\,w_\kappa\eta\,dx \;=:\; I_{21}+I_{22}. \end{aligned}$$

With (A.6) it follows that

(A.11)
$$\begin{aligned} I_{21} = &-\int_\Omega \eta\nabla\varrho\cdot\frac{\kappa}{|\nabla\varphi|}\Big(PD^2\varphi\nabla\varphi\nu^T+\nu\nabla\varphi^TD^2\varphi P\Big)\nabla\big(\Delta_\kappa\varrho\big)\,dx \\ &+\int_\Omega\eta\Big[P\nabla\varrho\cdot D^2(\Delta_\kappa\varrho)\kappa\nabla\varphi+P\nabla(\Delta_\kappa\varrho)\cdot D^2\varrho\kappa\nabla\varphi\Big]\,dx. \end{aligned}$$

With (A.3) we next compute

(A.12)
$$\begin{aligned} I_3 &= \int_\Omega\big(\Delta_\kappa\varrho\big)\nabla\cdot\big(e_\kappa\delta_\varphi P(\eta)\nabla\varrho\big)\,dx \\ &= -\int_\Omega\big(\Delta_\kappa\varrho\big)\nabla\cdot\left(e_\kappa\frac{1}{|\nabla\varphi|}\Big((\nu\cdot\nabla\varrho)P\nabla\eta+(\nabla\eta\cdot P\nabla\varrho)\nu\Big)\right)\,dx \\ &= \int_\Omega e_\kappa P\nabla(\Delta_\kappa\varrho)\cdot\frac{1}{|\nabla\varphi|}(\nu\cdot\nabla\varrho)\nabla\eta\,dx+\int_\Omega\nabla(\Delta_\kappa\varrho)\cdot\frac{e_\kappa}{|\nabla\varphi|}\big(\nabla\eta\cdot P\nabla\varrho\big)\nu\,dx \\ &=: I_{31}+I_{32}; \end{aligned}$$

further, by a partial integration and by (A.5)

(A.13)
$$\begin{aligned} I_{31} &= -\int_\Omega(\Delta_\kappa^2\varrho)\frac{e_\kappa}{|\nabla\varphi|}(\nu\cdot\nabla\varrho)\eta\,dx-\int_\Omega e_\kappa P\nabla(\Delta_\kappa\varrho)\cdot\nabla\left(\frac{1}{|\nabla\varphi|}(\nu\cdot\nabla\varrho)\right)\eta\,dx \\ &= -\int_\Omega(\Delta_\kappa^2\varrho)\frac{e_\kappa}{|\nabla\varphi|}(\nu\cdot\nabla\varrho)\eta\,dx-\int_\Omega e_\kappa P\nabla(\Delta_\kappa\varrho) \\ &\quad\cdot\left[\frac{1}{|\nabla\varphi|^2}\Big(\mathrm{Id}-2\nu\nu^T\Big)D^2\varphi\nabla\varrho\,+\frac{1}{|\nabla\varphi|}D^2\varrho\,\nu\right]\eta\,dx. \end{aligned}$$

Finally, we have by (A.4), (A.5)

(A.14)
$$\begin{aligned} I_{32} &= -\int_\Omega\eta\frac{e_\kappa}{|\nabla\varphi|}\Big[\nu\cdot D^2\big(\Delta_\kappa\varrho\big)P\nabla\varrho+\Big(\nu\cdot\nabla(\Delta_\kappa\varrho)\Big)\Big((\nabla\cdot P)\cdot\nabla\varrho+P:D^2\varrho\Big)\Big]\,dx \\ &\quad-\int_\Omega\eta e_\kappa\nabla(\Delta_\kappa\varrho)\cdot\frac{1}{|\nabla\varphi|^2}\Big(\mathrm{Id}-2\nu\nu^T\Big)D^2\varphi P\nabla\varrho\,dx \\ &\quad-\int_\Omega\eta\frac{1}{|\nabla\varphi|}\big(\nabla(\Delta_\kappa\varrho)\cdot\nu\big)\left(\kappa D^2\varphi\nabla\varphi+\frac{1}{\kappa}G'(\varphi)\nabla\varphi\right)\cdot P\nabla\varrho\,dx. \end{aligned}$$

For the L^2-gradient of the second-order part of the $\mathcal{F}^\kappa_{PFC}$ energy, we thus obtain from (A.9)–(A.14), using (A.7) in (A.14),

(A.15)

$$
\begin{aligned}
&\partial_\varphi \left(\int_\Omega \frac{1}{2} \big(\Delta_\kappa \varrho\big)^2 e_\kappa \, dx \right) \\
&\quad = \big(\Delta_\kappa \varrho\big) \nabla \big(\Delta_\kappa \varrho\big) \cdot \kappa \nabla \varphi - \frac{1}{2} \big(\Delta_\kappa \varrho\big)^2 w_\kappa \, - \, \nabla \varrho \cdot \kappa \Big(P D^2 \varphi \nu \nu^T + \nu \nu^T D^2 \varphi P \Big) \nabla \big(\Delta_\kappa \varrho\big) \\
&\qquad + P \nabla \varrho \cdot D^2 (\Delta_\kappa \varrho) \kappa \nabla \varphi + P \nabla (\Delta_\kappa \varrho) \cdot D^2 \varrho \kappa \nabla \varphi \, - \, P \nabla \big(\Delta_\kappa \varrho\big) \cdot \nabla \varrho \, w_\kappa \\
&\qquad - (\Delta_\kappa^2 \varrho) \frac{e_\kappa}{|\nabla \varphi|} (\nu \cdot \nabla \varrho) \, - \, e_\kappa P \nabla (\Delta_\kappa \varrho) \cdot \left[\frac{1}{|\nabla \varphi|^2} \Big(\mathrm{Id} - 2 \nu \nu^T \Big) D^2 \varphi \nabla \varrho \, + \frac{1}{|\nabla \varphi|} D^2 \varrho \, \nu \right] \\
&\qquad - \frac{e_\kappa}{|\nabla \varphi|} \left[\nu \cdot D^2 \big(\Delta_\kappa \varrho\big) P \nabla \varrho + \Big(\nu \cdot \nabla (\Delta_\kappa \varrho) \Big) \left(- \frac{\nabla \varrho}{|\nabla \varphi|} \cdot \Big(\mathrm{Id} - 2 \nu \nu^T \Big) D^2 \varphi \nu \right. \right. \\
&\qquad \left. \left. - \frac{1}{|\nabla \varphi|} \Delta \varphi (\nu \cdot \nabla \varrho) + P : D^2 \varrho \right) \right] \, - \, e_\kappa \nabla (\Delta_\kappa \varrho) \cdot \frac{1}{|\nabla \varphi|^2} \Big(\mathrm{Id} - 2 \nu \nu^T \Big) D^2 \varphi P \nabla \varrho \\
&\qquad - \frac{1}{|\nabla \varphi|} \big(\nabla (\Delta_\kappa \varrho) \cdot \nu \big) \left(\kappa D^2 \varphi \nabla \varphi + \frac{1}{\kappa} G'(\varphi) \nabla \varphi \right) \cdot P \nabla \varrho \\
&\quad = - \frac{1}{2} \big(\Delta_\kappa \varrho\big)^2 w_\kappa - \, P \nabla \big(\Delta_\kappa \varrho\big) \cdot \nabla \varrho \, w_\kappa - \, P \nabla (\Delta_\kappa \varrho) \cdot \frac{e_\kappa}{|\nabla \varphi|^2} D^2 \varphi \nabla \varrho \\
&\qquad - \Big(\mathrm{Id} - 2 \nu \nu^T \Big) \nabla (\Delta_\kappa \varrho) \cdot \frac{e_\kappa}{|\nabla \varphi|^2} D^2 \varphi P \nabla \varrho + [\nabla \big(\Delta_\kappa \varrho\big) \cdot \nu] \big(\Delta_\kappa \varrho\big) \kappa |\nabla \varphi| \\
&\qquad - [\nabla \big(\Delta_\kappa \varrho\big) \cdot \nu] \nabla \varrho \cdot \kappa P D^2 \varphi \nu - \, [\nabla \varrho \cdot \nu] \nu \cdot \kappa D^2 \varphi P \nabla \big(\Delta_\kappa \varrho\big) - \, [\nu \cdot \nabla \varrho] (\Delta_\kappa^2 \varrho) \frac{e_\kappa}{|\nabla \varphi|} \\
&\qquad + [\nu \cdot \nabla (\Delta_\kappa \varrho)] \frac{e_\kappa}{|\nabla \varphi|^2} \nabla \varrho \cdot \Big(\mathrm{Id} - 2 \nu \nu^T \Big) D^2 \varphi \nu + [\nu \cdot \varrho] [\nu \cdot \nabla (\Delta_\kappa \varrho)] \frac{e_\kappa}{|\nabla \varphi|^2} \Delta \varphi \\
&\qquad - [\nu \cdot \nabla (\Delta_\kappa \varrho)] \frac{e_\kappa}{|\nabla \varphi|} P : D^2 \varrho - \, [\nabla (\Delta_\kappa \varrho) \cdot \nu] \kappa D^2 \varphi \nu \cdot P \nabla \varrho \\
&\qquad + \left[\kappa |\nabla \varphi| - \frac{e_\kappa}{|\nabla \varphi|} \right] \Big(\nu \cdot D^2 \big(\Delta_\kappa \varrho\big) P \nabla \varrho + P \nabla (\Delta_\kappa \varrho) \cdot D^2 \varrho \nu \Big) \\
&\quad \approx - \frac{1}{2} \big(\Delta_\kappa \varrho\big)^2 w_\kappa - \, \nabla \big(\Delta_\kappa \varrho\big) \cdot \nabla \varrho \, w_\kappa - \, 2 \nabla (\Delta_\kappa \varrho) \cdot \kappa D^2 \varphi \nabla \varrho,
\end{aligned}
$$

where in the last line we have used that to lowest order of κ we have that $\varrho, \Delta_\kappa \varrho$ are constant in the normal direction and that we have to lowest order in κ equipartition of energy.

Next we consider the first-order term in $\mathcal{F}^\kappa_{PFC}$ and compute the variational derivative in the direction of a variation field $\eta \in C^\infty_c(\Omega)$:

(A.16)

$$
\begin{aligned}
\delta_\varphi \left(\int_\Omega |P \nabla \varrho|^2 \, e_\kappa \, dx \right) (\eta) \, &= \, \int_\Omega |P \nabla \varrho|^2 \delta_\varphi e_\kappa(\eta) \, dx + 2 P \nabla \varrho \cdot \delta_\varphi P(\eta) \nabla \varrho \, e_\kappa \, dx \\
&= \int_\Omega |P \nabla \varrho|^2 \big(\nabla \cdot (\kappa \eta \nabla \varphi) + w_\kappa \eta \big) \, dx - 2 \int_\Omega (\nu \cdot \nabla \varrho) P \nabla \varrho \cdot \nabla \eta \, \frac{e_\kappa}{|\nabla \varphi|} \, dx \\
&= \int_\Omega \eta |P \nabla \varrho|^2 w_\kappa \, dx - \int_\Omega 2 \eta P \nabla \varrho \cdot \partial_k (P \nabla \varrho) \kappa \partial_k \varphi \, dx \\
&\quad + 2 \int_\Omega \eta \nabla \cdot \left((\nu \cdot \nabla \varrho) P \nabla \varrho \frac{e_\kappa}{|\nabla \varphi|} \right) dx.
\end{aligned}
$$

For the L^2-gradient we therefore obtain by similar calculations as above that

$$\begin{aligned}
\partial_\varphi \left(\int_\Omega |P\nabla\varrho|^2 \, e_\kappa \, dx \right) &= |P\nabla\varrho|^2 w_\kappa + 2\frac{\kappa}{|\nabla\varphi|} P\nabla\varrho \cdot (\nu\cdot\nabla\varrho) P D^2\varphi \nabla\varphi \\
&\quad - 2P\nabla\varrho\cdot\kappa P D^2\varrho\nabla\varphi + 2\nabla\left(\frac{1}{|\nabla\varphi|}(\nu\cdot\nabla\varrho)\right)\cdot P\nabla\varrho\, e_\kappa \\
&\quad + 2\frac{e_\kappa}{|\nabla\varphi|}(\nu\cdot\nabla\varrho)\Delta_\kappa\varrho \\
&= |P\nabla\varrho|^2 w_\kappa + 2(\nu\cdot\nabla\varrho) P\nabla\varrho\cdot\kappa D^2\varphi\nu - 2P\nabla\varrho\cdot\kappa P D^2\varrho\nabla\varphi \\
&\quad + 2\left[\frac{1}{|\nabla\varphi|^2}\Big(\mathrm{Id} - 2\nu\nu^T\Big) D^2\varphi\nabla\varrho + \frac{1}{|\nabla\varphi|} D^2\varrho\,\nu\right]\cdot P\nabla\varrho e_\kappa \\
&\quad + 2\frac{e_\kappa}{|\nabla\varphi|}(\nu\cdot\nabla\varrho)\Delta_\kappa\varrho \\
&\approx |\nabla\varrho|^2 w_\kappa - 2\kappa|\nabla\varphi|\nabla\varrho\cdot D^2\varrho\nu + 2\frac{e_\kappa}{|\nabla\varphi|^2}\nabla\varrho\cdot D^2\varphi\nabla\varrho \\
&\quad + 2\frac{e_\kappa}{|\nabla\varphi|} D^2\varrho\,\nu\cdot\nabla\varrho \\
&\approx |\nabla\varrho|^2 w_\kappa + 2\nabla\varrho\cdot\kappa D^2\varphi\nabla\varrho, \qquad \text{(A.17)}
\end{aligned}$$

where we again have used that to lowest order normal derivatives of ϱ and $|\nabla\varrho|^2$ vanish and that to lowest order equipartition of energy holds.

Finally, we compute the variational derivative of the zeroth-order term in the diffuse PFC energy,

$$\delta_\varphi \left(\int_\Omega f(\varrho)\, e_\kappa \, dx \right)(\eta) \;=\; \int_\Omega f(\varrho)\delta_\varphi e_\kappa(\eta)\, dx = \int_\Omega -\eta f'(\varrho)\nabla\varrho\cdot\kappa\nabla\varphi + \eta f(\varrho) w_\kappa,$$

and therefore

$$\partial_\varphi \left(\int_\Omega f(\varrho)\, e_\kappa \, dx \right) \;=\; -(\nabla\varrho\cdot\nu)\kappa|\nabla\varphi| f'(\varrho) + f(\varrho) w_\kappa \;\approx\; f(\varrho) w_\kappa. \qquad \text{(A.18)}$$

Putting together (A.15), (A.17), (A.18), we arrive at the approximation (5.1).

Appendix B. Variational derivatives: Sharp interface energies. The evolution of the n-dimensional surface $\Gamma \subset \mathbb{R}^{n+1}$ is based on the energy (see [18])

$$\mathcal{F}_{Helfrich}(\varrho,\Gamma) = \int_\Gamma \kappa_N(\varrho)(H - H_0(\varrho))^2 \, \mathrm{d}\mu(x). \qquad \text{(B.1)}$$

The PFC model on an n-dimensional surface $\Gamma \subset \mathbb{R}^{n+1}$ is based on the energy

$$\mathcal{F}_{PFC}(\varrho,\Gamma) = \int_\Gamma \left(-\|\nabla_\Gamma\varrho\|_\Gamma^2 + \frac{1}{2}(\Delta_\Gamma\varrho)^2 + f(\varrho) \right) \mathrm{d}\mu(x) \qquad \text{(B.2)}$$

for a number density ϱ and a potential $f(\varrho) = \frac{1}{2}(1-\varepsilon)\varrho^2 + \frac{1}{4}\varrho^4$ with a parameter $\varepsilon \in \mathbb{R}$.

In order to derive a dynamic model for both the density ϱ and the surface Γ from a gradient flow perspective, one needs functional derivatives of (B.1) and (B.2), which are computed in the following. Note that, since $\varrho(t,\cdot)$ is a function on $\Gamma(t)$, with a variation of Γ we also vary ϱ.

B.1. Geometric notation. We introduce some basic geometric notation. Our object of interest is a closed moving surface $\Gamma = \Gamma(t) \subset \mathbb{R}^{n+1}$ parametrized by a one parameter family of smooth embeddings $\varphi : M \times [0,T] \to \mathbb{R}^{n+1}$, where M denotes a smooth closed n-dimensional manifold. To be more precise, we have $\Gamma(t) = \varphi(M,t)$. We define the trivial immersion $\Phi : \Gamma \to \mathbb{R}^{n+1}$ through

$$\Phi(x) := x = (x_1, \dots, x_{n+1}) \quad \text{for} \quad x \in \Gamma. \tag{B.3}$$

In addition, we introduce the mapping $\phi : M \times [0,T] \to \Gamma$ by the relation $\varphi = \Phi \circ \phi$. We denote the Euclidean scalarproduct $x \cdot y = \sum_{i=1}^{n+1} x_i y_i$ for x, $y \in \mathbb{R}^{n+1}$. Local coordinates in M are denoted by $\xi^1, \dots, \xi^n$, and we denote corresponding derivatives by $\partial_{\xi^i} u = \frac{\partial u}{\partial \xi^i}$, $i = 1, \dots, n$, for a function $u : M \to \mathbb{R}$. On Γ, we obtain induced local coordinates $z^1, \dots, z^n$ via $z = \xi \circ \phi^{-1}$. The tangent space $\mathrm{T}_x\Gamma$ of the surface Γ at the point $x = \varphi(p,t) \in \Gamma(t)$ is spanned by $\partial_{\xi^1}\varphi, \dots, \partial_{\xi^n}\varphi$ in the "embedded" sense and by $\partial_{z^1}|_x, \dots, \partial_{z^n}|_x$ in the sense of derivations, and deviating from the previous sections, we denote by ν in this section the *inner* normal.

We further introduce $\gamma_{ij} := \partial_{\xi^i}\varphi \cdot \partial_{\xi^j}\varphi$ (pullback) and $g_{ij}(x) = \partial_{z^i}\Phi(x) \cdot \partial_{z^j}\Phi(x)$ such that $\gamma_{ij}(p,t) = g_{ij}(\phi(p,t))$, $p \in M$, holds. We define the coefficients g^{ij} of the inverse $(g^{ij}) := (g_{ij})^{-1}$ and $g := \det(g_{ij})$ (and accordingly for γ). For tangent vectors $v = v^i \partial_{\xi^i}\varphi = v^i \partial_{z^i}|_x$ and $w = w^i \partial_{\xi^i}\varphi = w^i \partial_{z^i}|_x$, we then have the metric

$$\langle v, w \rangle_\Gamma = g_{ij} v^i w^j = v^i w^j \partial_{\xi^i}\varphi \cdot \partial_{\xi^j}\varphi = v \cdot w. \tag{B.4}$$

For convenience, we will often use $\partial_i := \partial_{z^i}$, $i = 1, \dots, n$, in the following. The norm on $\mathrm{T}_x\Gamma$ is thus defined through $\|v\|_\Gamma := \sqrt{\langle v, v \rangle_\Gamma}$, and the second fundamental form is given by $h_{ij} = II(\partial_{\xi^i}\varphi, \partial_{\xi^j}\varphi) = -\partial_i \nu \cdot \partial_{\xi^j}\varphi$ with $II(u,v) = h_{ij} v^i w^j$. We define $\langle X, Y \rangle_{\Gamma,n+1} := \sum_{i=1}^{n+1} \langle X_i, Y_i \rangle_\Gamma$ for $X, Y \in (\mathrm{T}\Gamma)^{n+1}$. Thereby, a typical example of $X \in (\mathrm{T}\Gamma)^{n+1}$ is given by

$$X = \nabla_\Gamma \Phi = \begin{pmatrix} \nabla_\Gamma \Phi_1 \\ \vdots \\ \nabla_\Gamma \Phi_{n+1} \end{pmatrix}.$$

In addition, we define

$$\langle X, v \rangle_\Gamma = \langle v, X \rangle_\Gamma = \begin{pmatrix} \langle X_1, v \rangle_\Gamma \\ \vdots \\ \langle X_{n+1}, v \rangle_\Gamma \end{pmatrix} \in \mathbb{R}^{n+1}$$

for $X \in (\mathrm{T}\Gamma)^{n+1}$ and $v \in \mathrm{T}\Gamma$.

Furthermore, we need the shape operator S, which is given by $S_{ij} = g^{ik} h_{kj}$. The norm of S is defined through $\|S\| = \sqrt{\mathrm{tr}(SS^T)} = \sqrt{S_{ij} S_{ji}}$. The mean curvature we define through $H = \mathrm{tr} S = \sum_{i=1}^{n} \kappa_i$, with κ_i the principal curvatures. The Christoffel symbols are given by $\Gamma^k_{ij} = \frac{1}{2} g^{kl}(\partial_i g_{jl} + \partial_j g_{il} - \partial_l g_{ij})$. Furthermore, we will need the Weingarten equations, which read $\partial_i \nu = -S_{ij} \partial_j \Phi$.

We use the surface divergence $\nabla_\Gamma \cdot W = \frac{1}{\sqrt{g}} \partial_i (\sqrt{g} \eta^i)$ for a tangential vector field $W = \eta^i \partial_{\xi^i}\varphi$, the surface gradient $\nabla_\Gamma = g^{ij} \partial_{\xi^i}\varphi \partial_j$, the Laplacian $\Delta_\Gamma = \nabla_\Gamma \cdot \nabla_\Gamma = \frac{1}{\sqrt{g}} \partial_i (\sqrt{g} g^{ij} \partial_j) = g^{ij} \partial_{ij} - g^{ij} \Gamma^k_{ij} \partial_k$, and the following identities (see [37, 29]):

$$\Delta_\Gamma \Phi = H \nu, \tag{B.5}$$

$$\langle \nabla_\Gamma \Phi, \nabla_\Gamma \varrho \rangle_\Gamma = \nabla_\Gamma \varrho = g^{ij} \partial_i \varrho \partial_{\xi^j}\varphi. \tag{B.6}$$

Furthermore, we denote the Riemannian connection by D. The Hessian $\mathrm{Hess}\,\varrho : \mathrm{T}\Gamma \to \mathrm{T}\Gamma$ of a function $\varrho : \Gamma \to \mathbb{R}$ is defined as the covariant derivative of the gradient of ϱ,

$$(\mathrm{Hess}\,\varrho)Y := \mathrm{D}_Y \nabla_\Gamma \varrho \tag{B.7}$$

for a vector field $Y \in \mathrm{T}\Gamma$. Then one obtains

$$\langle \nabla_\Gamma \langle \nabla_\Gamma \varrho, \nabla_\Gamma \psi\rangle_\Gamma, \nabla_\Gamma \eta\rangle_\Gamma = \langle (\mathrm{Hess}\,\varrho)\nabla_\Gamma \eta, \nabla_\Gamma \psi\rangle_\Gamma + \langle \nabla_\Gamma \varrho, (\mathrm{Hess}\,\psi)\nabla_\Gamma \eta\rangle_\Gamma \tag{B.8}$$

for functions $\varrho, \psi, \eta : \Gamma \to \mathbb{R}$. In addition, the Hessian is symmetric:

$$\langle (\mathrm{Hess}\,\varrho)X, Y\rangle_\Gamma = \langle X, (\mathrm{Hess}\,\varrho)Y\rangle_\Gamma. \tag{B.9}$$

Furthermore, for a function $\varrho : \Gamma \to \mathbb{R}$, the integral of ϱ over Γ is given by

$$\int_{\Gamma(t)} \varrho(x)\,\mathrm{d}\mu(x) = \int_M \varrho(\varphi(p,t))\sqrt{\gamma(p,t)}\,\mathrm{d}\mu(p).$$

B.2. Basic variations. We provide the variational derivatives of $\mathcal{F}$ with respect to φ and ϱ. The calculations closely follow the approach in [37]. The basic strategy is to consider the derivative

$$\frac{\mathrm{d}}{\mathrm{d}t}\mathcal{F}(\varrho,\Gamma)\Big|_{t=0}$$

and represent the result of the derivative as

$$\frac{\mathrm{d}}{\mathrm{d}t}\mathcal{F}(\varrho,\Gamma)\Big|_{t=0} = \int_\Gamma \left(\partial_\Phi \mathcal{F}(\varrho(x,0),\Gamma(0))\cdot \frac{\mathrm{d}}{\mathrm{d}t}\Phi\Big|_{t=0} + \partial_\varrho \mathcal{F}(\varrho(x,0),\Gamma(0))\frac{\mathrm{d}}{\mathrm{d}t}\varrho\Big|_{t=0}\right)\mathrm{d}\mu(x),$$

which can be interpreted as the definition of the partial functional derivatives $\partial_\Phi \mathcal{F}$ and $\partial_\varrho \mathcal{F}$. Furthermore, we use the notation $\delta := \frac{\mathrm{d}}{\mathrm{d}t}\big|_{t=0}$.

In order to compute the variation of the energy we need the following variations.

LEMMA B.1.

$$\delta(\mathrm{d}\mu(\varphi(p,t))) = \delta(\sqrt{\gamma(p,t)}\,\mathrm{d}\mu(p)) = \langle \nabla_\Gamma \delta\Phi, \nabla_\Gamma \Phi\rangle_{\Gamma,n+1}\,\mathrm{d}\mu(x), \tag{B.10}$$

$$\delta(\gamma^{ij}(p,t)) = -g^{ki}\left(\partial_k \delta\Phi\cdot\partial_l\Phi + \partial_l\delta\Phi\cdot\partial_k\Phi\right)g^{lj}. \tag{B.11}$$

Proof. We only sketch the proof and follow the calculations in [37]. We use $\partial_i\Phi(x) = \partial_{\xi^i}\varphi(p,t)$ with $x = \varphi(p,t)$, the sum convention, and write

$$\delta\Phi = g^{ij}\delta\Phi\cdot\partial_i\Phi\partial_j\Phi + \delta\Phi\cdot\nu\nu. \tag{B.12}$$

One essential result that is needed is the variation of the metric

$$\delta g_{ij} = \partial_i\delta\Phi\cdot\partial_j\Phi + \partial_j\delta\Phi\cdot\partial_i\Phi. \tag{B.13}$$

For a differentiable matrix $A = A(t) \in \mathbb{R}^{n\times n}$ one has

$$\frac{\mathrm{d}}{\mathrm{d}t}\det A(t)\Big|_{t=0} = \det A(0)\mathrm{tr}\left(A(0)^{-1}\frac{\mathrm{d}}{\mathrm{d}t}A(t)\Big|_{t=0}\right).$$

Because of $\mathrm{d}\mu(\varphi(p,t)) = \sqrt{\det(\gamma_{ij})_{i,j}}\,\mathrm{d}\mu(p)$ we get

$$\begin{aligned}2\mathrm{d}\mu(\varphi(p,t))\delta(\mathrm{d}\mu(\varphi(p,t))) &= \delta(\det(\gamma_{ij})_{i,j})\,\mathrm{d}\mu(p) = \det((\gamma_{ij})_{i,j})\gamma^{ij}\delta\gamma_{ij}\,\mathrm{d}\mu(p)\\ &= \gamma^{ij}(\partial_{\xi^i}\delta\varphi\cdot\partial_{\xi^j}\varphi + \partial_{\xi^j}\delta\varphi\cdot\partial_{\xi^i}\varphi)\mathrm{d}\mu(\varphi(p,t)),\end{aligned}$$

which yields (B.10). The proof of (B.11) easily follows from (B.13). ∎

B.3. Variation of $\mathcal{F}_{Helfrich}$. The derivation of the functional derivatives of the Helfrich energy can be found, e.g., in [37, 29, 17] for H_0 and κ_N constant.

B.3.1. Variation of the normal bending energy. In the case of the normal bending energy, one obtains

$$\begin{aligned}
&\frac{\mathrm{d}}{\mathrm{d}t}\mathcal{F}_{Helfrich,B}(\varrho,\Gamma)\Big|_{t=0}\\
&= \int_\Gamma \Delta_\Gamma(\kappa_N(\varrho)(H-H_0(\varrho)))\delta\Phi\cdot\nu\,\mathrm{d}\mu(x) + \int_\Gamma \kappa_N(\varrho)(H-H_0(\varrho))\|S\|^2\delta\Phi\cdot\nu\,\mathrm{d}\mu(x)\\
&\quad - \frac{1}{2}\int_\Gamma \kappa_N(\varrho)(H-H_0(\varrho))^2 H\delta\Phi\cdot\nu\,\mathrm{d}\mu(x)\\
&\quad + \int_\Gamma \frac{1}{2}\kappa_N'(\varrho)(H-H_0(\varrho))\delta\varrho\,\mathrm{d}\mu(x) - \int_\Gamma \kappa_N(\varrho)(H-H_0(\varrho))H_0'(\varrho)\delta\varrho\,\mathrm{d}\mu(x)\\
&\quad - \frac{1}{2}\int_\Gamma \kappa_N'(\varrho)(H-H_0(\varrho))^2\langle\nabla_\Gamma\varrho,\nabla_\Gamma\Phi\rangle_\Gamma\cdot\delta\Phi\,\mathrm{d}\mu(x)\\
&\quad + \int_\Gamma \kappa_N(\varrho)(H-H_0(\varrho))H_0'(\varrho)\langle\nabla_\Gamma\varrho,\nabla_\Gamma\Phi\rangle_\Gamma\cdot\delta\Phi\,\mathrm{d}\mu(x)
\end{aligned}$$

and therefore partial functional derivatives

$$\begin{aligned}
\partial_\Phi\mathcal{F}_{Helfrich,B}(\varrho(x,0),\Gamma(0)) &= \Delta_\Gamma(\kappa_N(\varrho)(H-H_0(\varrho)))\nu\\
&\quad + \kappa_N(\varrho)(H-H_0(\varrho))\|S\|^2\nu - \frac{1}{2}\kappa_N(\varrho)(H-H_0(\varrho))^2H\nu\\
&\quad - \frac{1}{2}\kappa_N'(\varrho)(H-H_0(\varrho))^2\nabla_\Gamma\varrho + \kappa_N(\varrho)(H-H_0(\varrho))H_0'(\varrho)\nabla_\Gamma\varrho,\\
\partial_\varrho\mathcal{F}_{Helfrich,B}(\varrho(x,0),\Gamma(0)) &= \frac{1}{2}\kappa_N'(\varrho)(H-H_0(\varrho)) - \kappa_N(\varrho)(H-H_0(\varrho))H_0'(\varrho).
\end{aligned}$$

B.4. Variation of $\mathcal{F}_{PFC}$. For a computation of a functional derivative of a Ginzburg–Landau free energy on a surface, we refer to [17].

B.4.1. Variation of the zero-order term. We define

$$\mathcal{F}_{PFC,0}(\varrho,\Gamma) := \int_\Gamma f(\varrho)\,\mathrm{d}\mu(x)$$

and obtain as an intermediate result

$$\frac{\mathrm{d}}{\mathrm{d}t}\mathcal{F}_{PFC,0}(\varrho,\Gamma)\Big|_{t=0} = \int_\Gamma f'(\varrho)\delta\varrho\,\mathrm{d}\mu(x) + \int_\Gamma f(\varrho)\langle\nabla_\Gamma\delta\Phi,\nabla_\Gamma\Phi\rangle_{\Gamma,n+1}\,\mathrm{d}\mu(x), \tag{B.14}$$

which is part of the basis for a weak formulation, with $\delta\varrho$ and $\delta\Phi$ being the test functions. Furthermore, we compute

$$\begin{aligned}
\frac{\mathrm{d}}{\mathrm{d}t}\mathcal{F}_{PFC,0}(\varrho,\Gamma)\Big|_{t=0} &= \int_\Gamma f'(\varrho)\delta\varrho\,\mathrm{d}\mu(x) - \int_\Gamma f(\varrho)\delta\Phi\cdot\Delta_\Gamma\Phi\,\mathrm{d}\mu(x)\\
&\quad - \int_\Gamma f'(\varrho)\nabla_\Gamma\varrho\cdot\delta\Phi\,\mathrm{d}\mu(x)\\
&= \int_\Gamma f'(\varrho)\delta\varrho\,\mathrm{d}\mu(x) - \int_\Gamma f(\varrho)H\nu\cdot\delta\Phi\,\mathrm{d}\mu(x)\\
&\quad - \int_\Gamma f'(\varrho)\nabla_\Gamma\varrho\cdot\delta\Phi\,\mathrm{d}\mu(x),
\end{aligned}$$

where we have used (B.6). In other words,

$$\begin{aligned}\partial_\Phi \mathcal{F}_{PFC,0}(\varrho(x,0),\Gamma(0)) &= -f(\varrho)H\nu - f'(\varrho)\nabla_\Gamma \varrho,\\ \partial_\varrho \mathcal{F}_{PFC,0}(\varrho(x,0),\Gamma(0)) &= f'(\varrho).\end{aligned}$$

B.4.2. Variation of the first-order term. We define

$$\mathcal{F}_{PFC,1}(\varrho,\Gamma) := \frac{1}{2}\int_\Gamma \|\nabla_\Gamma \varrho\|_\Gamma^2 \,\mathrm{d}\mu(x) = \frac{1}{2}\int_\Gamma g^{ij}\partial_i\varrho\partial_j\varrho\,\mathrm{d}\mu(x)$$

and compute

$$\begin{aligned}\frac{1}{2}(\delta g^{ij})\partial_i\varrho\partial_j\varrho &= -\frac{1}{2}g^{ki}\left(\partial_k\delta\Phi\cdot\partial_l\Phi + \partial_l\delta\Phi\cdot\partial_k\Phi\right)g^{lj}\partial_i\varrho\partial_j\varrho\\ &= -\langle\nabla_\Gamma\delta\Phi,\nabla_\Gamma\varrho\rangle_\Gamma\cdot\langle\nabla_\Gamma\Phi,\nabla_\Gamma\varrho\rangle_\Gamma,\end{aligned}$$

and we obtain as an intermediate result

$$\frac{\mathrm{d}}{\mathrm{d}t}\mathcal{F}_{PFC,1}(\varrho,\Gamma)\Big|_{t=0} = -\int_\Gamma \langle\nabla_\Gamma\delta\Phi,\nabla_\Gamma\varrho\rangle_\Gamma\cdot\langle\nabla_\Gamma\Phi,\nabla_\Gamma\varrho\rangle_\Gamma\,\mathrm{d}\mu(x) \tag{B.15}$$

$$+\int_\Gamma \langle\nabla_\Gamma\delta\varrho,\nabla_\Gamma\varrho\rangle_\Gamma\,\mathrm{d}\mu(x) \tag{B.16}$$

$$+\int_\Gamma \frac{1}{2}\|\nabla_\Gamma\varrho\|_\Gamma^2\,\langle\nabla_\Gamma\delta\Phi,\nabla_\Gamma\Phi\rangle_{\Gamma,n+1}\,\mathrm{d}\mu(x), \tag{B.17}$$

which is part of the basis for a weak formulation. Furthermore, we finally get

$$\begin{aligned}&\frac{\mathrm{d}}{\mathrm{d}t}\mathcal{F}_{PFC,1}(\varrho,\Gamma)\Big|_{t=0}\\ &= -\int_\Gamma \langle\nabla_\Gamma\delta\Phi,\nabla_\Gamma\varrho\rangle_\Gamma\cdot\langle\nabla_\Gamma\Phi,\nabla_\Gamma\varrho\rangle_\Gamma\,\mathrm{d}\mu(x)\\ &\quad -\int_\Gamma \Delta_\Gamma\varrho\delta\varrho\,\mathrm{d}\mu(x) + \int_\Gamma \frac{1}{2}\|\nabla_\Gamma\varrho\|_\Gamma^2\,\langle\nabla_\Gamma\delta\Phi,\nabla_\Gamma\Phi\rangle_{\Gamma,n+1}\,\mathrm{d}\mu(x),\end{aligned}$$

and from this we obtain by (B.8) and (B.9)

$$\begin{aligned}&\partial_\Phi\mathcal{F}_{PFC,1}(\varrho(x,0),\Gamma(0))\\ &= \Delta_\Gamma\varrho\nabla_\Gamma\varrho + \langle\nabla_\Gamma\langle\nabla_\Gamma\varrho,\nabla_\Gamma\Phi\rangle_\Gamma,\nabla_\Gamma\varrho\rangle_\Gamma - \frac{1}{2}\langle\nabla_\Gamma\|\nabla_\Gamma\varrho\|_\Gamma^2,\nabla_\Gamma\Phi\rangle_\Gamma\\ &\quad -\frac{1}{2}\|\nabla_\Gamma\varrho\|_\Gamma^2 H\nu\\ &= \Delta_\Gamma\varrho\nabla_\Gamma\varrho + \langle(\text{Hess }\varrho)\nabla_\Gamma\varrho,\nabla_\Gamma\Phi\rangle_\Gamma + \langle\nabla_\Gamma\varrho,(\text{Hess }\Phi)\nabla_\Gamma\varrho\rangle_\Gamma\\ &\quad -\langle(\text{Hess }\varrho)\nabla_\Gamma\Phi,\nabla_\Gamma\varrho\rangle_\Gamma - \frac{1}{2}\|\nabla_\Gamma\varrho\|_\Gamma^2 H\nu\\ &= \Delta_\Gamma\varrho\nabla_\Gamma\varrho + \langle\nabla_\Gamma\varrho,(\text{Hess }\Phi)\nabla_\Gamma\varrho\rangle_\Gamma - \frac{1}{2}\|\nabla_\Gamma\varrho\|_\Gamma^2 H\nu.\end{aligned}$$

Furthermore, we get

$$\partial_\varrho\mathcal{F}_{PFC,1}(\varrho(x,0),\Gamma(0)) = -\Delta_\Gamma\varrho.$$

B.4.3. Variation of the second-order term. We define

$$\mathcal{F}_{PFC,2}(\varrho,\Gamma) := \int_\Gamma \frac{1}{2}(\Delta_\Gamma \varrho)^2 \,\mathrm{d}\mu(x).$$

Here, we need

$$\begin{aligned}
\delta\Delta_\Gamma\varrho &= \delta\left(\frac{1}{\sqrt{g}}\partial_i(\sqrt{g}g^{ij}\partial_j\varrho)\right)\\
&= -\frac{1}{g}\delta(\sqrt{g})\partial_i(\sqrt{g}g^{ij}\partial_j\varrho) + \frac{1}{\sqrt{g}}\partial_i(\delta(\sqrt{g})g^{ij}\partial_j\varrho)\\
&\quad + \frac{1}{\sqrt{g}}\partial_i(\sqrt{g}\delta(g^{ij})\partial_j\varrho) + \frac{1}{\sqrt{g}}\partial_i(\sqrt{g}g^{ij}\partial_j\delta\varrho)\\
&= -\frac{1}{\sqrt{g}}\langle\nabla_\Gamma\delta\Phi,\nabla_\Gamma\Phi\rangle_{\Gamma,n+1}\partial_i(\sqrt{g}g^{ij}\partial_j\varrho) + \frac{1}{\sqrt{g}}\partial_i(\langle\nabla_\Gamma\delta\Phi,\nabla_\Gamma\Phi\rangle_{\Gamma,n+1}\sqrt{g}g^{ij}\partial_j\varrho)\\
&\quad - \frac{1}{\sqrt{g}}\partial_i(\sqrt{g}g^{ki}\left(\partial_k\delta\Phi\cdot\partial_l\Phi + \partial_l\delta\Phi\cdot\partial_k\Phi\right)g^{lj}\partial_j\varrho) + \Delta_\Gamma\delta\varrho\\
&= -\langle\nabla_\Gamma\delta\Phi,\nabla_\Gamma\Phi\rangle_{\Gamma,n+1}\Delta_\Gamma\varrho + \nabla_\Gamma\cdot(\langle\nabla_\Gamma\delta\Phi,\nabla_\Gamma\Phi\rangle_{\Gamma,n+1}\nabla_\Gamma\varrho)\\
&\quad - \nabla_\Gamma\cdot(\nabla_\Gamma\delta\Phi\cdot\langle\nabla_\Gamma\Phi,\nabla_\Gamma\varrho\rangle_\Gamma + \langle\nabla_\Gamma\delta\Phi,\nabla_\Gamma\varrho\rangle_\Gamma\cdot\nabla_\Gamma\Phi) + \Delta_\Gamma\delta\varrho,
\end{aligned}$$

and we obtain as an intermediate result

$$\begin{aligned}
&\frac{\mathrm{d}}{\mathrm{d}t}\mathcal{F}_{PFC,2}(\varrho,\Gamma)\Big|_{t=0}\\
&\quad= -\int_\Gamma\langle\nabla_\Gamma\delta\Phi,\nabla_\Gamma\Phi\rangle_{\Gamma,n+1}(\Delta_\Gamma\varrho)^2\,\mathrm{d}\mu(x)\\
&\qquad -\int_\Gamma\langle\nabla_\Gamma\Delta_\Gamma\varrho,\nabla_\Gamma\varrho\rangle_\Gamma\langle\nabla_\Gamma\delta\Phi,\nabla_\Gamma\Phi\rangle_{\Gamma,n+1}\,\mathrm{d}\mu(x)\\
&\qquad +\int_\Gamma\langle\nabla_\Gamma\Delta_\Gamma\varrho,\nabla_\Gamma\delta\Phi\cdot\langle\nabla_\Gamma\Phi,\nabla_\Gamma\varrho\rangle_\Gamma + \langle\nabla_\Gamma\delta\Phi,\nabla_\Gamma\varrho\rangle_\Gamma\cdot\nabla_\Gamma\Phi\rangle_\Gamma\,\mathrm{d}\mu(x)\\
&\qquad +\int_\Gamma\Delta_\Gamma\varrho\Delta_\Gamma\delta\varrho\,\mathrm{d}\mu(x) + \frac{1}{2}\int_\Gamma(\Delta_\Gamma\varrho)^2\langle\nabla_\Gamma\delta\Phi,\nabla_\Gamma\Phi\rangle_{\Gamma,n+1}\,\mathrm{d}\mu(x),
\end{aligned}\tag{B.18}$$

which is part of the basis for a weak formulation. With this we obtain

$$\begin{aligned}
&\frac{\mathrm{d}}{\mathrm{d}t}\mathcal{F}_{PFC,2}(\varrho,\Gamma)\Big|_{t=0}\\
&= \int_\Gamma\delta\Phi\cdot\Delta_\Gamma\Phi(\Delta_\Gamma\varrho)^2\,\mathrm{d}\mu(x) + 2\int_\Gamma\delta\Phi\cdot\langle\nabla_\Gamma\Phi,\nabla_\Gamma\Delta_\Gamma\varrho\rangle_\Gamma\Delta_\Gamma\varrho\,\mathrm{d}\mu(x)\\
&\quad +\int_\Gamma\langle\nabla_\Gamma\Delta_\Gamma\varrho,\nabla_\Gamma\varrho\rangle_\Gamma\delta\Phi\cdot\Delta_\Gamma\Phi\,\mathrm{d}\mu(x)\\
&\quad +\int_\Gamma\langle\nabla_\Gamma\langle\nabla_\Gamma\Delta_\Gamma\varrho,\nabla_\Gamma\varrho\rangle_\Gamma,\nabla_\Gamma\Phi\rangle_\Gamma\cdot\delta\Phi\,\mathrm{d}\mu(x)\\
&\quad -\int_\Gamma\Delta_\Gamma^2\varrho\delta\Phi\cdot\langle\nabla_\Gamma\Phi,\nabla_\Gamma\varrho\rangle_\Gamma\,\mathrm{d}\mu(x)\\
&\quad -\int_\Gamma\delta\Phi\cdot\langle\nabla_\Gamma\Delta_\Gamma\varrho,\nabla_\Gamma\langle\nabla_\Gamma\Phi,\nabla_\Gamma\varrho\rangle_\Gamma\rangle_\Gamma\,\mathrm{d}\mu(x)\\
&\quad -\int_\Gamma\delta\Phi\cdot\langle\nabla_\Gamma\Delta_\Gamma\varrho,\nabla_\Gamma\Phi\rangle_\Gamma\Delta_\Gamma\varrho\,\mathrm{d}\mu(x)
\end{aligned}$$

$$
\begin{aligned}
&- \int_\Gamma \delta\Phi \cdot \langle \nabla_\Gamma \langle \nabla_\Gamma \Delta_\Gamma \varrho, \nabla_\Gamma \Phi\rangle_\Gamma, \nabla_\Gamma \varrho\rangle_\Gamma \,\mathrm{d}\mu(x) \\
&+ \int_\Gamma \Delta_\Gamma^2 \varrho \delta\varrho \,\mathrm{d}\mu(x) - \frac{1}{2}\int_\Gamma (\Delta_\Gamma \varrho)^2 \delta\Phi \cdot \Delta_\Gamma \Phi \,\mathrm{d}\mu(x) \\
&- \int_\Gamma \Delta_\Gamma \varrho \langle \nabla_\Gamma \Delta_\Gamma \varrho, \nabla_\Gamma \Phi\rangle_\Gamma \cdot \delta\Phi \,\mathrm{d}\mu(x).
\end{aligned}
$$

From this one gets

$$
\begin{aligned}
&\partial_\Phi \mathcal{F}_{PFC,2}(\varrho(x,0),\Gamma(0)) \\
&= \frac{1}{2}(\Delta_\Gamma \varrho)^2 H\nu + \langle \nabla_\Gamma \Delta_\Gamma \varrho, \nabla_\Gamma \varrho\rangle_\Gamma H\nu + \langle \nabla_\Gamma \langle \nabla_\Gamma \Delta_\Gamma \varrho, \nabla_\Gamma \varrho\rangle_\Gamma, \nabla_\Gamma \Phi\rangle_\Gamma \\
&\quad - \Delta_\Gamma^2 \varrho \langle \nabla_\Gamma \Phi, \nabla_\Gamma \varrho\rangle_\Gamma - \langle \nabla_\Gamma \Delta_\Gamma \varrho, \nabla_\Gamma \langle \nabla_\Gamma \Phi, \nabla_\Gamma \varrho\rangle_\Gamma\rangle_\Gamma \\
&\quad - \langle \nabla_\Gamma \langle \nabla_\Gamma \Delta_\Gamma \varrho, \nabla_\Gamma \Phi\rangle_\Gamma, \nabla_\Gamma \varrho\rangle_\Gamma \\
&= \frac{1}{2}(\Delta_\Gamma \varrho)^2 H\nu + \langle \nabla_\Gamma \Delta_\Gamma \varrho, \nabla_\Gamma \varrho\rangle_\Gamma H\nu + \langle (\mathrm{Hess}\ \Delta_\Gamma \varrho)\nabla_\Gamma \varrho, \nabla_\Gamma \Phi\rangle_\Gamma \\
&\quad + \langle (\mathrm{Hess}\ \varrho)\nabla_\Gamma \Delta_\Gamma \varrho, \nabla_\Gamma \Phi\rangle_\Gamma - \Delta_\Gamma^2 \varrho \langle \nabla_\Gamma \Phi, \nabla_\Gamma \varrho\rangle_\Gamma \\
&\quad - \langle \nabla_\Gamma \Delta_\Gamma \varrho, (\mathrm{Hess}\ \Phi)\nabla_\Gamma \varrho\rangle_\Gamma - \langle \nabla_\Gamma \Delta_\Gamma \varrho, (\mathrm{Hess}\ \varrho)\nabla_\Gamma \Phi\rangle_\Gamma \\
&\quad - \langle (\mathrm{Hess}\ \Delta_\Gamma \varrho)\nabla_\Gamma \Phi, \nabla_\Gamma \varrho\rangle_\Gamma - \langle (\mathrm{Hess}\ \Phi)\nabla_\Gamma \Delta_\Gamma \varrho, \nabla_\Gamma \varrho\rangle_\Gamma \\
&= \frac{1}{2}(\Delta_\Gamma \varrho)^2 H\nu + \langle \nabla_\Gamma \Delta_\Gamma \varrho, \nabla_\Gamma \varrho\rangle_\Gamma H\nu - 2\langle (\mathrm{Hess}\ \Phi)\nabla_\Gamma \Delta_\Gamma \varrho, \nabla_\Gamma \varrho\rangle_\Gamma \\
&\quad - \Delta_\Gamma^2 \varrho \langle \nabla_\Gamma \Phi, \nabla_\Gamma \varrho\rangle_\Gamma.
\end{aligned}
$$

Furthermore,

$$
\partial_\varrho \mathcal{F}_{PFC,2}(\varrho(x,0),\Gamma(0)) = \Delta_\Gamma^2 \varrho.
$$

B.4.4. Variation of total PFC energy. For the variations of the total PFC energy

$$
\mathcal{F}_{PFC}(\varrho,\Gamma) = \mathcal{F}_{PFC,0}(\varrho,\Gamma) - 2\mathcal{F}_{PFC,1}(\varrho,\Gamma) + \mathcal{F}_{PFC,2}(\varrho,\Gamma)
$$

one has to sum up the corresponding variations of the energies $\mathcal{F}_{PFC,i}$, $i = 0, 1, 2$.

REFERENCES

[1] A. Agrawal and D. J. Steigmann, *A model for surface diffusion of transmembrane proteins on lipid bilayers*, Z. Angew. Math. Phys., 62 (2011), pp. 549–563.

[2] S. Aland, J. Lowengrub, and A. Voigt, *A continuum model of colloid-stabilized interfaces*, Phys. Fluids, 23 (2011), 062103.

[3] R. Backofen, M. Gräf, D. Potts, S. Praetorius, A. Voigt, and T. Witkowski, *A continuous approach to discrete ordering on* $\mathbb{S}^2$, Multiscale Model. Simul., 9 (2011), pp. 314–334.

[4] R. Backofen, A. Voigt, and T. Witkowski, *Particles on curved surfaces: A dynamic approach by a phase-field-crystal model*, Phys. Rev. E, 81 (2010), 025701.

[5] A. R. Bausch, M. J. Bowick, A. Cacciuto, A. D. Dinsmore, M. F. Hsu, D. R. Nelson, M. G. Nikolaides, A. Travesset, and D. A. Weitz, *Grain boundary scars and spherical crystallography*, Science, 299 (2003), pp. 1716–1718.

[6] M. Bowick and L. Giomi, *Two-dimensional matter: Order, curvature and defects*, Adv. Phys., 58 (2009), pp. 449–563.

[7] R. Bruinsma, W. Gelbert, D. Reguera, J. Rudnick, and R. Zandi, *Viral self-assembly as a thermodynamic process*, Phys. Rev. Lett., 90 (2003), 248101.

[8] D. L. D. Caspar and A. Klug, *Physical principles in construction of regular viruses*, in Proceedings of the Cold Spring Harbor Symposia on Quantitative Biology, Vol. 27, Cold Spring Harbor Laboratory Press, Woodbury, NJ, 1962, pp. 1–24.

[9] E. De Giorgi, *Some remarks on Γ-convergence and least squares method*, in Composite Media and Homogenization Theory (Trieste, 1990), Progr. Nonlinear Differential Equations Appl. 5, Birkhäuser Boston, Boston, MA, 1991, pp. 135–142.
[10] D. E. Discher and A. Eisenberg, *Self-assembled aggregates of rod-coil block copolymers and their solublilization and encapsulation of fullerenes*, Science, 279 (1998), pp. 1903–1907.
[11] D. E. Discher and A. Eisenberg, *Polymer vesicles*, Science, 297 (2002), pp. 967–973.
[12] A. Disnmore, M. Hsu, M. Nikolaides, M. Marquez, A. Bausch, and D. Weitz, *Colloidosomes: Selectively permeable capsules composed of colloidal particles*, Science, 298 (2002), pp. 1006–1009.
[13] Q. Du, C. Liu, and X. Wang, *A phase field approach in the numerical study of the elastic bending energy for vesicle membranes*, J. Comput. Phys., 198 (2004), pp. 450–468.
[14] K. Elder, M. Haataja, and M. Grant, *Modeling elasticity in crystal growth*, Phys. Rev. Lett., 88 (2002), 245701.
[15] K. Elder, M. Katakowski, M. Haataja, and M. Grant, *Modeling elasticity in crystal growth*, Phys. Rev. Lett., 88 (2002), 245701.
[16] K. R. Elder, N. Provatas, J. Berry, P. Stefanovic, and M. Grant, *Phase-field crystal modeling and classical density functional theory of freezing*, Phys. Rev. B, 75 (2007), 064107.
[17] C. Elliott and B. Stinner, *Modeling and computation of two phase geometric biomembranes using surface finite elements*, J. Comput. Phys., 229 (2010), pp. 6585–6612.
[18] W. Helfrich, *Elastic properties of lipid bilayers—Theory and possible experiments*, Z. Naturforsch. C, 28 (1973), pp. 693–701.
[19] L. Jia, A. Cao, D. Levy, B. Xu, P. A. Albouy, X. Xing, M. J. Bowick, and M. H. Li, *Smectic polymer vesicles*, Soft Matter, 5 (2009), pp. 3446–3451.
[20] T. Kohyama and G. Gompper, *Defect scars on flexible surfaces with crystalline order*, Phys. Rev. Lett., 98 (2007), 198101.
[21] J. Lidmar, L. Mirny, and D. R. Nelson, *Virus shapes and buckling transitions in spherical shells*, Phys. Rev. E, 68 (2003), 051910.
[22] J. Lowengrub, A. Rätz, and A. Voigt, *Phase-field modeling of the dynamics of multicomponent vesicles: Spinodal decomposition, coarsening, budding, and fission*, Phys. Rev. E, 79 (2009), 031926.
[23] H. McMahon and J. Gallop, *Membrane curvature and mechanisms of dynamic cell membrane remodelling*, Nature, 438 (2005), pp. 590–596.
[24] L. Modica, *The gradient theory of phase transitions and the minimal interface criterion*, Arch. Ration. Mech. Anal., 98 (1987), pp. 357–383.
[25] L. Modica and S. Mortola, *Un esempio di Γ-convergenza*, Boll. Un. Mat. Ital. B (5), 14 (1977), pp. 285–299.
[26] A. G. Murzin, S. E. Brenner, T. Hubbard, and C. Chothia, *SCOP: A structural classification of proteins database for the investigation of sequences and structures*, J. Molecular Biol., 247 (1995), pp. 537–540.
[27] A. Rätz and A. Voigt, *PDEs on surfaces—A diffuse interface approach*, Comm. Math. Sci., 4 (2006), pp. 575–590.
[28] M. Röger and R. Schätzle, *On a modified conjecture of De Giorgi*, Math. Z., 254 (2006), pp. 675–714.
[29] R. Rusu, *An algorithm for the elastic flow of surfaces*, Interfaces Free Bound., 7 (2005), pp. 229–239.
[30] U. Seifert, *Configurations of fluid membranes and vesicles*, Adv. Phys., 46 (1997), pp. 13–137.
[31] K. Stratford, R. Adhikari, I. Pagonabarraga, J. Desplat, and M. Cates, *Colloidal jamming at interfaces: A route to fluid-bicontinuous gels*, Science, 309 (2005), pp. 2198–2201.
[32] S. van Teeffelen, R. Backofen, A. Voigt, and H. Löwen, *Derivation of the phase-field-crystal model for colloidal solidification*, Phys. Rev. E, 79 (2009), 051404.
[33] J. Thomson, *On the structure of the atom: An investigation of the stability and periods of oscillation of a number of corpuscles arranged at equal intervals around the circumference of a circle; with application of the results to the theory of atomic structure,* Philos. Mag. Ser. 6, 7 (1904), pp. 237–265.
[34] A. Turner, V. Vitelli, and D. Nelson, *Vortices on curved surfaces*, Rev. Modern Phys., 82 (2010), pp. 1301–1348.
[35] R. Verfürth, *A Review of A Posteriori Error Estimation and Adaptive Mesh-Refinement Techniques*, Wiley-Teubner Ser. Adv. Numer. Math., John Wiley & Sons, Chichester, B. G. Teubner, Stuttgart, 1996.

[36] S. Vey and A. Voigt, *AMDiS: Adaptive multidimensional simulations*, Comput. Vis. Sci., 10 (2007), pp. 57–67.
[37] T. J. Willmore, *Riemannian Geometry*, Oxford Science Publications, The Clarendon Press, Oxford University Press, New York, 1993.
[38] J. Yang, R. Pinol, F. Gubelline, D. Levy, P. A. Albouy, P. Keller, and M. H. Li, *Formation of polymer vesicles by liquid crystal amphiphilic block copolymers*, Langmuir, 22 (2006), pp. 7907–7911.